

Wright State University

CORE Scholar

[Browse all Theses and Dissertations](#)

[Theses and Dissertations](#)

2021

Functionalizing Ceramic Matrix Composites by the Integration of a Metallic Substructure with Comparable Feature Size

Elizabeth Pierce Heckman
Wright State University

Follow this and additional works at: https://corescholar.libraries.wright.edu/etd_all



Part of the [Engineering Science and Materials Commons](#)

Repository Citation

Heckman, Elizabeth Pierce, "Functionalizing Ceramic Matrix Composites by the Integration of a Metallic Substructure with Comparable Feature Size" (2021). *Browse all Theses and Dissertations*. 2471.
https://corescholar.libraries.wright.edu/etd_all/2471

This Thesis is brought to you for free and open access by the Theses and Dissertations at CORE Scholar. It has been accepted for inclusion in Browse all Theses and Dissertations by an authorized administrator of CORE Scholar. For more information, please contact library-corescholar@wright.edu.

FUNCTIONALIZATING CMCs BY THE INTEGRATION OF A METALLIC
SUBSTRUCTURE WITH COMPARABLE FEATURE SIZE

A Thesis submitted in partial fulfillment of the
requirements for the degree of
Master of Science in Material Science and Engineering

by

ELIZABETH PIERCE HECKMAN
B.S.M.S.E, Wright State University, 2020

2021

Wright State University

APPROVAL FOR PUBLIC RELEASE

CASE NUMBER: AFRL-2021-1480

WRIGHT STATE UNIVERSITY
GRADUATE SCHOOL

April 16th, 2021

I HEREBY RECOMMEND THAT THE THESIS PREPARED UNDER MY
SUPERVISION BY Elizabeth Pierce Heckman ENTITLED Functionalizing CMCs by
the Integration of a Metallic Substructure with Comparable Feature Size BE ACCEPTED
IN PARTIAL FULFILLMENT OF THE REQUIREMENTS FOR THE DEGREE OF
Master of Science in Material Science and Engineering.

Hong Huang, Ph.D.
Thesis Director

Raghavan Srinivasan, Ph.D.,
P.E.
Chair, Mechanical and Materials
Engineering Department

Committee on Final Examination:

Hong Huang, Ph.D.

Joy Gockel, Ph.D.

Zlatomir Apostolov, Ph.D.

Barry Milligan, Ph.D.
Vice Provost for Academic Affairs
Dean of the Graduate School

ABSTRACT

Heckman, Elizabeth Pierce. M.S.M.S.E., Department of Mechanical and Materials Engineering, Wright State University, 2021. Functionalizing CMCs by the Integration of a Metallic Substructure with Comparable Feature Size.

A metallic network has been embedded in a silicon carbide fiber– silicon carbide (SiC) matrix ceramic composite (CMC) in order to combine the functional properties of the metal and the structural properties of the CMC. The processing of the composite involves iterative pre-ceramic polymer infiltration and heating to temperatures at 1100°C. The metallic structure embedded in the CMC must retain its unique properties during processing and cannot convert to a silicide or carbide resulting from diffusion of Si and C species from the SiC matrix. To gain an understanding of the diffusion process, a fully processed CMC with tungsten, tantalum, and molybdenum wires will be heated at various temperatures for the same duration. The diffusion zone will be measured and then kinetics equations will be applied to determine the failure kinetics. Understanding the diffusion kinetics and phases formed at higher temperature can provide a processing path which avoids metal degradation.

Contents

1. Introduction	1
1.1 What Are Ceramic Matrix Composites?.....	1
1.2 CMC Processing Methods	4
1.3 Polymer Infiltration Pyrolysis (PIP)	4
1.4 SiC/SiC CMCs	8
1.5 Metal – CMC System Joining Process	10
1.6 Metal – CMC Composite Integration	12
1.7 Metal Selective Criteria in the Metal – CMC Composite Integration	14
1.8 Outline of this Thesis	15
2. Theory	17
2.1 Carbides and Silicides of Ta, W, and Mo	17
2.1.1 Phase Diagrams.....	17
2.2 Past Experimental Studies.....	21
2.3. Diffusion	32
2.3.1. Arrhenius Equation	32
2.3.1. Experimental Example	33
3. Analysis Methods.....	35
3.1 Scanning Electron Microscopy	35
3.2 Energy Dispersive Spectroscopy	36
3.3 Raman Spectroscopy.....	37
4. Processing and Characterizations of “Mock” CMCs.....	39
4.1 Experimental Aspects.....	40
4.1.1 Layup	40
4.1.2 Processing of Refractory Wires and “Mock” CMC	44
4.1.3 Sectioning and Metallography Preparation	49
4.1.4 SEM and EDS Characterizations	50
4.2 Results and Discussion	51
4.3 Conclusions	57

5. Processing and Characterization of the 1100°C CMC	59
5.1 Experimental Aspects.....	60
5.1.1 Layup	60
5.1.2 Processing	62
5.1.3 Sectioning and Metallography Preparation	63
5.1.4 SEM and EDS Analyses	64
5.2 Results and Discussion	64
5.3 Conclusion.....	67
6. Si and C Diffusion Study in a CMC at High Temperatures.....	69
6.1 Experimental Methodology	71
6.1.1 Layup	71
6.1.2 Processing	73
6.1.3 Sectioning and Metallography Preparation	76
6.2 Results	76
6.3 Conclusion.....	92
7. Summary and Conclusions	94
7.1 Summary	94
7.2 Conclusions	95
7.2.1 “Mock” CMC.....	95
7.2.2 1100°C CMC.....	96
7.2.3 Diffusion Study.....	96
7.3 Significance of Results.....	97
7.4 Future Work	98
References	101

List of Figures

Figure 1: Different fiber orientations within a CMC. (a) unidirectional, (b) random, (c) bidirectional, and (d) multi-directional; Source: [1].....	2
Figure 2: Slurry for coating the fiber weaves (left); Fiber weave coated in slurry and the roller used to press it into the individual fibers (right).	5
Figure 3: Vacuum bagging materials necessary for the temperature range of 177°C to 202°C.	6
Figure 4: The overall process for creating a CMC through PIP processing; Source: [4]. ..	8
Figure 5: Different SiC structures; [7].	9
Figure 6: Integration of a metallic substrate into the CMC; [Zlatomir Apostolov].....	13
Figure 7: Phase diagram for silicon and tantalum; [14].....	18
Figure 8: Phase Diagram for silicon and tungsten; [15].	18
Figure 9: Phase Diagram for silicon and molybdenum; [16].....	19
Figure 10: The tantalum carbon phase diagram; [18].....	20
Figure 11: The tungsten carbon phase diagram; [19].	20
Figure 12: The molybdenum carbon phase diagram; [20].....	21
Figure 13: The Mo-Si-C system ternary phase diagram as determined by Brewer in 1956; [22].	26
Figure 14: The Ta-Si-C system ternary phase diagram as determined by Brewer in 1956; [22].	26
Figure 15: The W-Si-C system ternary phase diagram as determined by Brewer in 1956; [22].	27
Figure 16: The metal foils, type of silicon carbide, final temperature, applied pressure, and overall bond quality of the relevant studies in Cockeram's research; [23].	28
Figure 17: The SiC/Mo/SiC system after heating; [23].	29

Figure 18: The tungsten diffusion path in the SiC/W/SiC system; [23].	30
Figure 19: The diffusion path overlayed on the W-Si-C ternary phase diagram; [23].	31
Figure 20: The potential interactions after the incident electrons hit the surface of the sample; [25].	35
Figure 21: The “mock” CMC layup process.	41
Figure 22: The weighted plate resting on the “mock” CMC to prevent movement when the vacuum is pulled.	42
Figure 23: The fully vacuumed bagged plate with the thermocouple and vacuum ports attached to the plate.	43
Figure 24: The plate loaded into the autoclave with the thermocouples attached, the vacuum hoses attached, and the vacuum pulled.	44
Figure 25: All of the “mock” CMC samples with the iterative PIP processing cycles associated with each sample.	49
Figure 26: The section portion of the “mock” CMC before being placed in epoxy.	50
Figure 27: SEM images of the three metal wires after five cycles of heating at 900°C.	51
Figure 28: SEM images of the 1100°C “mock” CMC wires after processing.	52
Figure 29: The tungsten wire SEM image, carbon EDS map, and silicon EDS map from the mock CMC after processing at 1300°C.	52
Figure 30: The molybdenum wire SEM image and the silicon EDS map from the mock CMC after five cycles at 1300°C, showing the reaction region within the wire.	53
Figure 31: The tantalum wire SEM image from the mock CMC after five iterative cycles at 1300°C, showing no signs of degradation.	54
Figure 32: The tungsten wire after the additional 1500°C pyrolysis. The left side of the carbon EDS map shows the major metal to matrix separation.	55
Figure 33: The molybdenum wire after the additional 1500°C pyrolysis. There is a non-uniform reaction zone.	55
Figure 34: The tantalum wire after the additional 1500°C pyrolysis. There is not any metal to matrix fusion present around the wire.	55
Figure 35: The tungsten wire after the additional 1700°C pyrolysis.	56
Figure 36: The molybdenum wire after the additional 1700°C pyrolysis.	56

Figure 37: The tantalum wire after the additional 1700°C pyrolysis.....	57
Figure 38: The overall stability of the wires at the different processing temperatures.....	58
Figure 39: The difference between warp and weft fiber weave orientation; [27].	61
Figure 40: The interface of each sample that was cut and analyzed using SEM and EDS.	63
Figure 41: EDS maps of Tantalum and molybdenum 250 micron wires after the 7th PIP cycle showing metal expansion and change from the original circular shape of the wires.	64
Figure 42: The final EDS maps taken for each wire after eight cycles of PIP processing.	67
Figure 43: The fiber weaves after B-staging and being prepared for freezer storage.....	72
Figure 44: The final CMC layup of the 1100°C CMC.	72
Figure 45: The final CMC layup schematic.....	73
Figure 46: The CMC in the SMP-10 during reinfiltration.	74
Figure 47: The CMC after the reinfiltration and ready for the vacuum oven to cure the SMP-10 in place in the pores.....	75
Figure 48: A model of how the CMC was sectioned after the additional 1500°C heating cycles.	77
Figure 49: The tantalum wire after four additional heating cycles to 1500°C.....	78
Figure 50: The tungsten wire after four additional heating cycles to 1500°C.	79
Figure 51: The tantalum wire EDS linescan after four cycles of the additional 1500°C. The red line represents that tantalum signal, and the light blue line represents the silicon signal.	79
Figure 52: The tungsten wire EDS linescan after four cycles of the additional 1500°C. The green line represents that tungsten signal, and the light blue line represents the silicon signal.	80
Figure 53: The silicon diffusion into the molybdenum wire after two hours of additional heating.	81
Figure 54: The linescan from the molybdenum wire after one hour of additional heating to 1500°C. The red line represents the silicon signal, and the light blue line represents the molybdenum signal.	81

Figure 55: The linescan from the molybdenum wire after two hours of additional heating to 1500°C. The red line represents the silicon signal, and the green line represents the molybdenum signal.	82
Figure 56: The linescan from the molybdenum wire after three hours of additional heating to 1500°C. The red line represents the silicon signal, and the purple line represents the molybdenum signal.	82
Figure 57: The linescan from the molybdenum wire after four hours of additional heating to 1500°C. The red line represents the silicon signal, and the green line represents the molybdenum signal.	83
Figure 58: The differences in diffusion zone thickness within one sample (1500°C/4h).	85
Figure 59: The time dependency plot for the diffusion thickness versus time.	86
Figure 60: The molybdenum wire right section MatLab code to overlay all five data sets together.	87
Figure 61: The MatLab generated intensity versus position graph between the fiber and matrix scan showing the differences in the carbon content.....	88
Figure 62: The carbon peaks resulting in positive intensity reading.	89
Figure 63: The noise in the data resulting in negative intensity reading.	89
Figure 64: Two different Raman spectroscopy scans that include fiber carbon intensity. The image on the left is the molybdenum wire after 1100°C x 8 and the image on the right is the molybdenum wire after 1100°C x 8 + 1500°C x 4.	90
Figure 65: Two different Raman spectroscopy scans that include matrix carbon intensity. The image on the left is the tungsten wire after 1100°C x 8 + 1500°C x 2 and the image on the right is the tantalum wire after 1100°C x 8 + 1500°C x 4.	90
Figure 66: The molybdenum wire bottom region Raman spectroscopy data.	91
Figure 67: The tantalum wire right region Raman spectroscopy data.	91
Figure 68: The tungsten wire top region Raman spectroscopy data.	92

List of Tables

Table 1: The autoclave processing parameters for the “mock” CMCs.....	44
Table 2: The iterative pyrolysis processing parameters for the 900°C processed wires. .	45
Table 3: The 1st pyrolysis processing parameters for the 1100°C “mock” CMCs.	46
Table 4: The 1st pyrolysis processing parameters for the 1300°C “mock” CMCs.	46
Table 5: The iterative processing parameters for the vacuum oven.	47
Table 6: The iterative pyrolysis processing parameters for the 1100°C “mock” CMCs..	47
Table 7: The iterative pyrolysis processing parameters for the 1300°C “mock” CMCs..	47
Table 8: The additional pyrolysis processing parameters for the 1300°C 250 micron “mock” CMCs.	48
Table 9: The additional pyrolysis processing parameters for the 1300°C 500 micron “mock” CMCs.	48
Table 10: The 1st cycle graphite furnace processing parameters.	74
Table 11: The iterative vacuum oven curing run.	75
Table 12: The additional 1500°C processing parameters.	76

Acknowledgements

I would like to thank all of my advisors for their constant support, expertise in the subject, and guidance as I completed my thesis. Thank you to Dr. Zlatomir Apostolov, who guided me through four years of work at AFRL and provided me with the best start in my career as an engineer. Thank you to Dr. Hong Huang, who always went out of her way to ensure I was succeeding, in her classes, with my thesis, and in life. Thank you to Dr. Joy Gockel, who was the first professor I felt a connection with at Wright State. Her class was the first class where I felt like I could actually succeed as an engineer.

I would also like to thank my friends and family. Without their constant support and encouragement, I would not have published this paper. Thank you to my mother, Rebecca Heckman, who always answered my calls and told me I could do it and to keep pushing. Thank you to my father, Steven Heckman, who always made me feel smarter than I actually am when I talked about school and my work. Thank you to my brother, John Heckman, who always made me forget about the stress of school. Thank you to all of my aunts, uncles, cousins, and grandparents who always met me with smiling faces and good food on the Sundays I could make it back down to Cincinnati. I love you all.

A special thank you to my best friend, Bridget Larson, who never left my side and was always there to bounce ideas off of. Without you, I could not have made it through college. Bridget was there at my first job at AFRL and now we get to work together again post-graduation, which is the biggest gift. You were there at the start and I know you will always be there.

Finally, I would like to thank my Grandma Heckman, who passed away in December of 2020. Even though you were not there to see me graduation, I know you were there with me the whole time. I love you and I miss you.

1. Introduction

The objective of this research is the integration of metallic substrates into a ceramic matrix composite (CMC). The purpose of this is to combine the structural properties of the CMC with the functional properties of the metallic substrate in a singular component. The metallic substrate cannot add significant cost to the processing of the CMC, the properties of the substrate cannot be degraded due to CMC processing, and the addition of the substrate cannot have a detrimental effect on the properties inherent to the CMC. Before a functional CMC could be produced, background data was necessary. One key fundamental data will be the overall diffusion characteristics of the ceramic matrix into the metallic substrate during CMC processing. This information will allow for the determination of the phases present within the metal and then the overall properties associated with each phase. This research was conducted at the Wright Patterson Air Force Base in the Air Force Research Laboratories.

1.1 What Are Ceramic Matrix Composites?

Ceramic matrix composites (CMCs) consist of multiple ceramic phases added together to achieve better overall properties associated with the individual ceramic phases. The addition of one or more ceramic phases can assist an individual monolithic ceramic in increased properties. Often properties that are targeted and manipulated by adding different ceramic phases are various chemical, thermal, electrical, and mechanical properties. The basic form of the constituents of CMCs are a primary ceramic phase,

acting as the matrix, and a secondary ceramic phase that is embedded in the primary ceramic matrix. The secondary ceramic phases are often ceramic fibers or particulates. There are multiple different orientations that the fibers can be embedded in the matrix; unidirectional, bidirectional, random, and multi-directional. The different fiber orientations can be seen in Figure 1. Each fiber orientation has its own benefits and the overall orientation depends of the application and properties needed for each individual CMC [2].

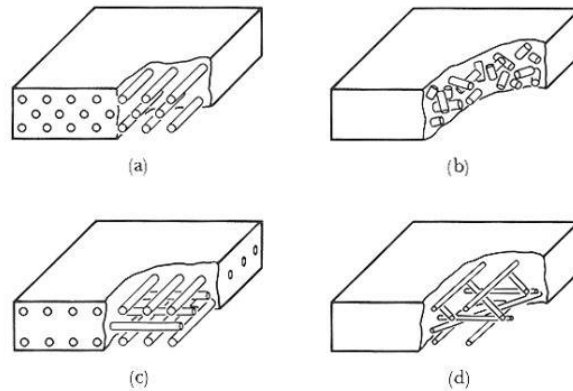


Figure 1: Different fiber orientations within a CMC. (a) unidirectional, (b) random, (c) bidirectional, and (d) multi-directional; Source: [1].

Common ceramic fibers and particulates that are used in CMCs are silicon carbide (SiC) and silicon nitride (Si_3N_4) fibers. Carbon fibers are also very commonly used in CMCs. The matrix material, or the primary ceramic phase, is often alumina (Al_2O_3), silicon carbide, titanium carbide (TiC), silicon nitride, and many other different types of ceramics; including some various glasses [2].

Normally ceramics are very strong but have brittle behavior, resulting in catastrophic failure. The fiber and particulates embedded in the matrix act as reinforcements for the

ceramic matrix, thus increasing the mechanical properties by reducing the catastrophic failure associated with the ceramic matrix. A careful combination of the brittle ceramic constituents can result in a CMC that has excellent mechanical and thermal properties, as well as being very damage resistant. Overall, CMCs have very high temperature resistance and have good wear resistance. The lightweight properties and ability to survive in very harsh environments, make CMCs great contenders for aerospace applications. The high mechanical strengths and thermal properties make them sound thermostructural materials suitable for applications in the automotive industry, aerospace industry, and chemical industries. Some specific applications for CMCs include leading edges, gas turbines, heat exchangers, and heat engines. Leading edges are nozzle tips or wing tips on aircraft. These parts of the aircraft experience very high pressures and temperatures due to the overall friction of the air against the part. Due to this, the leading edge material has to be something that is extremely thermally resistant and exhibits excellent mechanical properties [3]. The specific applications and properties for each type of CMC is dependent on the processing methods and the constituents, specifically the fiber reinforcements, matrix, and the interfaces/interphases associated with the joining of the fibers and the matrix [4].

Originally, the majority of the research being done on CMCs were focusing on the processing methods. Current research of CMCs is focused on more of the properties associated with CMCs. Some of these properties include high temperature stability in aggressive environments, such as turbine engines, the overall lifespan of the CMC, predictive failure models, and simulations during flight or overall use [4].

1.2 CMC Processing Methods

There are three main processing methods for CMCs, which are polymer infiltration pyrolysis (PIP), chemical vapor infiltration (CVI), and melt infiltration (MI). The process used during the fabrication of the CMCs used in this experiment was PIP processing.

1.3 Polymer Infiltration Pyrolysis (PIP)

Polymer infiltration pyrolysis (PIP) processing can be broken down into four specific steps. Preparation of fibers, manufacturing of a fiber reinforced preform, pyrolysis of the fiber reinforced preform, and then densification of the fiber reinforced preform through multiple cycles of polymer infiltration pyrolysis. The preparation of the fibers includes the spinning and deposition of the coating on the fiber. The specific chemistry of the fiber and the coating depends on the specific type of CMC to be made and the specific application and properties needed. The manufacturing of the fiber reinforced preform is typically done through fiber lay ups. To lay up the fiber weaves, a slurry is needed to bind the fiber weaves together. The slurry consists of a ceramic powder that will be the matrix and a pre-ceramic polymer that will also become the matrix. The pre-ceramic polymer should have a backbone that is similar to the ceramic powder so that the polymer can be turned into a ceramic during the pyrolysis steps later on during the processing. Figure 2 shows a typical layup process that involves coating the fiber weaves with the slurry mixture and then stacking the fiber weaves on top of each other.



Figure 2: Slurry for coating the fiber weaves (left); Fiber weave coated in slurry and the roller used to press it into the individual fibers (right).

The orientation, shape, size, and amount of the fiber weaves is dependent on the type of ceramic matrix composite and the overall properties and applications needed. The number of fiber weaves stacked together is also dependent on the overall application for the eventual CMC [4, 5].

Another way that the fiber weaves can be prepared for the layup process is by B-staging the weaves. There are three official stages of polymers during reinfiltration, A-stage, B-stage, and C-stage. A-stage is when the polymer exhibits no cross-linking and C-stage is when the polymer is fully cross-linked. B-stage occurs when the degree of cross-linking varies within the polymer and the rigidity of the polymer is also varied. B-staging is very useful because it allows for polymers to partially gel within the fiber weaves and allows for better control over the polymer behavior. B-staging of a fiber weave occurs by heating the infiltrated weave, done by rolling the polymer into the weave as mentioned above, at a temperature below the curing point of the polymer being used. This allows for the fiber weave to still be pliable and conformable to whatever shape is necessary but prevents cracks and fiber loss while laying up the weaves [5].

Once the fiber reinforced preform has been manufactured, the pyrolysis of the preform is next. Preceding the pyrolysis, the fiber reinforced preform is vacuum bagged. This process is very lengthy and involves multiple different types of tape, plastics, and bagging film. Once the preform is bagged, it is connected to an autoclave. The autoclave applies a specific pressure and a specific temperature. The purpose of the autoclave is to initially cure the CMC. The CMC will be extremely brittle and not fully transitioned into a ceramic. The autoclave can be programmed for specific runs, characteristic to the specific needs of each individual type of ceramic matrix composite, and for specific amounts of time, commonly between one hour to three hours. Figure 3 shows the common set up for a vacuum bagged CMC that is prepared for a cycle in an autoclave [4, 5].

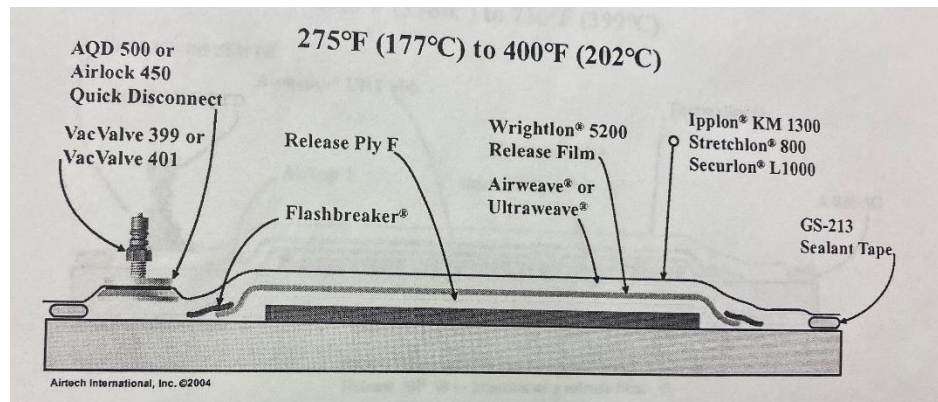


Figure 3: Vacuum bagging materials necessary for the temperature range of 177°C to 202°C.

After the initial curing in the autoclave is complete, the fiber reinforced preform is placed in a graphite furnace for the first initial pyrolysis cycle. This pyrolysis cycle turned the fiber reinforced preform into a densified ceramic matrix composite. The pyrolysis temperature for the graphite furnace is again dependent on the specific needs for the finalized ceramic matrix composite. The typically temperature range is anywhere between 1100°C to 1600°C. After the first pyrolysis is finished, the resultant CMC is very

porous. The porosity inside the CMC is not ideal as it serves as an initial place for crack propagations. To remedy this situation, the polymer infiltration pyrolysis method is used. The same pre-ceramic polymer that was used in the slurry is used to densify and close the pores present in the CMC. This is done by placing the CMC under vacuum and a container of the pre-ceramic polymer under vacuum. A tube with needles attached to either side are placed into the vacuum containers and the pressure difference causes the pre-ceramic polymer to flow through the tube into the vacuum container with the CMC in it. The pre-ceramic polymer then flows into the pores within the CMC. This process typically runs for about an hour or two and then the CMC is placed into a vacuum furnace to cure the pre-ceramic polymer within the pores. The temperature that the vacuum furnace operate at is dependent on the pre-ceramic polymer and its overall cure temperature. After the pre-ceramic polymer is cured in the pores, the CMC is run through another cycle of pyrolysis to turn the pre-ceramic polymer into a ceramic, thus densifying the ceramic matrix composite and reducing the overall porosity. This process is repeated for about five to nine cycles. The process is stopped once the CMC reaches less than two percent weight gain [4, 5]. Figure 4 shows the overall process for creating a CMC through PIP processing.

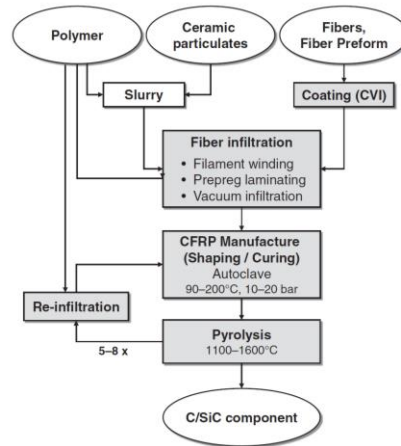


Figure 4: The overall process for creating a CMC through PIP processing; Source: [4].

The PIP processing is very well defined so there is not much research being done to help expedite this process. However, there is some research that revolves around the PIP processing, specifically the pre-ceramic polymers that are used in the process. The ceramics and ceramic matrix composite division at the Air Force Research Laboratory is focusing on research involving the heat treatment of the pre-ceramic polymers before use in the PIP processing cycle. By heat treated the pre-ceramic polymers, low molecular weight oligomers could be released from the polymer chain before use in the PIP processing. This could potentially result in higher ceramic yield, which would be ideal for CMCs. Various different methods of heat treating the polymers have been investigated and various methods of determining the changes to the pre-ceramic polymer chains have been analyzed, such as thermogravimetric analysis, gel permeation chromatography, differential scanning calorimeter, and rheological characterization [5, 6].

1.4 SiC/SiC CMCs

The main constituents of silicon carbide – silicon carbide CMCs are silicon carbide powder, SMP-10, a silicon carbide backbone pre-ceramic polymer, and silicon

carbide fibers with various coatings. Some of the fibers that often used are Hi-Nicalon, Hi-Nicalon Type S, Tyranno SA3, and Sylramic fibers. Each of these fibers have slightly different chemistries, processing methods, coatings, and properties. There are multiple different types of crystalline structures of silicon carbide and each different structure has slightly different properties associated with it. The two most common structures of silicon carbide that are seen in SiC/SiC CMCs are α -SiC and β -SiC. The β -SiC takes a cubic 3C form while the α -SiC takes either a hexagonal 4H or hexagonal 6H form. Figure 5 shows the different stacking sequences of the different silicon carbide structures [4, 7].

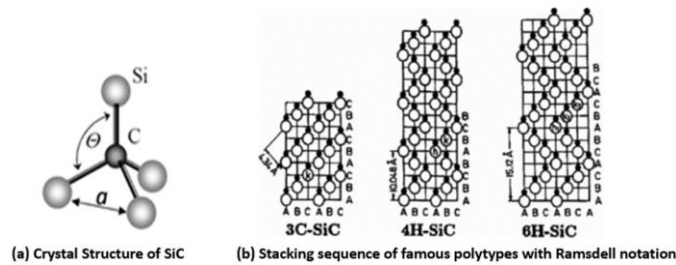
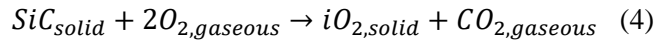
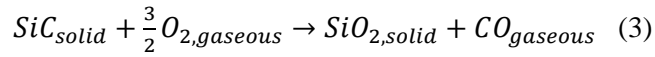
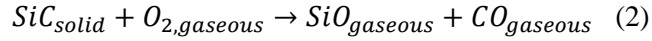
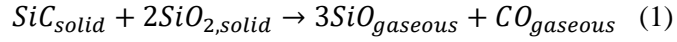


Figure 5: Different SiC structures; [7].

Overall, the properties associated with ceramic matrix composites change depending on the processing method and the specific constituents. SiC/SiC ceramic matrix composites have very high mechanical strengths, thermal resistance, thermal conductivity, electrical conductivity, and oxidation resistance. The majority of the research that is occurring around silicon carbide – silicon carbide CMCs is focusing on determining the specific properties associated with the different processing methods and the individual laminate layers of the CMC [8]. Other research is focusing on the determination of the SiC/SiC CMCs in oxidizing environments. Once a SiC/SiC CMC is at temperature above 900°C, there are two different types of oxidation it can experience, either active or passive. Active oxidation is defined in Equations 1 and 2 while passive oxidation is defined in Equations 3 and 4 [9]. By analyzing these equations and running experimental tests, like

done by Nasiri, oxidation layers and overall weight gain can be measured for the CMCs, determining the overall oxidation behavior at specific temperatures.



NASA Glenn in Cleveland is one of the leading the research in the applications of silicon carbide – silicon carbide ceramic matrix composites. The Ultra Efficiency Engine Technology (UEET) Program is investigating the CMCs for low-emission engine systems and propulsion engines, such as inlet turbine vanes [10]. Other research that is being done at NASA Glenn in Cleveland is for the Next Generation Launch Technology (NGLT) Program. They are investigating the potential uses of silicon carbide – silicon carbide CMCs for reusable launch vehicle propulsion and airframe applications. The materials being investigated are silicon carbide – silicon carbide CMCs due to the lightweight properties associated with them. This will increase the overall efficiency of the vehicle. The enhanced mechanical and thermal properties will increase the overall safety and the low manufacturing cost will help reduce overall project cost [11].

1.5 Metal – CMC System Joining Process

The joining of a processed CMC to another part is something that introduces a source of failure into the overall system, however the CMC is relatively useless unless it can be joined to existing parts. The typical process of welding the two parts together is not feasible since the CMC cannot be welded. There are a few processes that have been used in industry to join the CMC to other parts including adhesives, fasteners, screw/nut systems, and bolt/riev systems. For the joining of one CMC to another part, metallic

parts are not used because the metals cannot operate at the required temperature for the overall system. The joining processes are typically made of a composite material or another CMC. Some examples of integration methods include composite fasteners, round braided CMC fasteners, and CMC “T” joints. These integration methods have some disadvantages associated with them, including coefficient of thermal expansion mismatch between the fasteners and the parts and overall stress concentrations at the point of joining. However, these joining methods are also favorable due to the easy assembly of the combined parts. Adhesion of the parts is not done when the new component is to operate at high temperatures. This is due to the adhesives having low melting points and not being suitable for extreme temperature environments. The only time adhesive methods are used to join a CMC and another part is when the CMC is being joined to a polymer. Current studies are focusing on adhesives that have a high melting temperature and overall working temperature; however, they are not currently used in industry to join a CMC to another part [4].

The most common joining method for CMCs to another metallic part is brazing. Brazing involves alloys being melted down and acting as a metallic glue to hold two parts together. The alloy is placed either as a foil or a paste between the CMC and the other part. It is then heated above its liquidus temperature. The alloy that is chosen has to have a melting temperature that is much lower than the melting temperature of the CMC and the metallic part being joined together. Common brazing alloys are copper, silver, and nickel. Gold and aluminum are also used for very specific purposes. The copper, silver, and nickel brazing alloys are typically used to join a CMC to a nickel-based superalloy or a cobalt-based superalloy. There are some issues with the brazing method of joining a

CMC to a metallic part. There is the issue of wettability of the CMC and the part being joined, the overall reactivity of the parts being joined together, and the overall thermal stability of the alloy used at temperature. If the alloy has low thermodynamic stability, then the issue of diffusion between the brazing alloy and the parts joined together arises. Brazing alloys are great ways to join CMCs to other CMCs or a CMC to a metallic structure. However, if the conditions of wettability, reactivity, and thermodynamic stability between the brazing alloy and the parts being joined together are not considered, the joined material will experience failure. When all of these parameters are accounted for, successful joints, both continuous and uniform, can be made between a CMC and a metallic part [4]. These methods all detailed the joining of a CMC to a metallic part. The objective of this research is to combine a CMC with a metallic substrate to help the overall functionality of the CMC. CMCs are mostly used in structural applications and the research involving CMCs and metals are in the exterior joining methods. This research focused on the joining of CMCs and metals together, within the composite.

1.6 Metal – CMC Composite Integration

The integration of metals into the CMC can be done in a few different ways. The metals can be introduced into the matrix of the CMC as particulates, wires, or sheets of metal. This project is focusing on the integration of the metals as wires. The wires were chosen in hopes of being able to have a comparable feature size to the matrix within the CMC. **Error! Reference source not found.** shows the planned metallic wire integrated within the CMC.

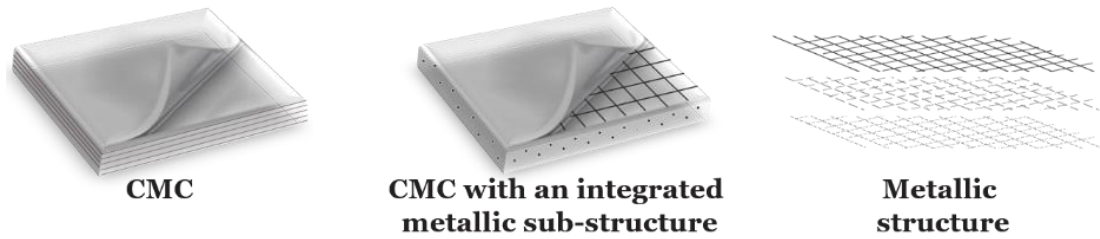


Figure 6: Integration of a metallic substrate into the CMC; [Zlatomir Apostolov].

There are some potential properties and applications associated with the integration of metallic wires within the CMC. Potential properties could be introduced to the CMC from the metal. These could include electrical conductance, thermal conductance, and magnetic abilities. By introducing these functional properties to the CMC, it would allow for the CMC to not only be used as a structural component. If the electrical or thermal conductance is improved within the CMC, then potential failure data and failure predictions could be utilized. The metal wires could serve as a failure predictor.

Measurements of the overall electric conductance of the CMC could be tested throughout operation. There could potentially be a correlation between the electrical conductance readings and when the CMC is likely to fail.

The above mentioned potential failure predictions need to be validated with data, so the main objective of this research is to create the CMC with the metallic substrate and test how it survives the overall CMC processing. There will be a significant amount of diffusion from the silicon carbide matrix into the metallic substrate. This will cause a change in phases present within the wires to include silicides and carbides. Once the phases present are determined, the properties can be associated to the phases. The properties associated with the phases will then directly correlate to the properties associated to the CMC. Testing will then be done to the CMC to see if a failure prediction method is actually something that can be applied to the CMC. The testing will take place

far in the future, so the analysis of the phases present within the CMC is the main objective.

1.7 Metal Selective Criteria in the Metal – CMC Composite Integration

Refractory metals were investigated for the integration of metallic substrates in CMCs because they have extremely high melting and operating temperatures. The high melting point can be attributed to the character and high strength of the interatomic bonds. The melting temperatures for the refractory metals are higher than the common CMC operating temperatures, meaning they could be utilized in the CMC, theoretically, without the metallic substrate degrading during operation. Refractory metals are also extremely resistant to overall wear. Refractory metals have excellent electrical resistance. This characteristic would allow for the metals to be tested before use and during use. The values of electrical resistance could be used to determine how long the CMC has left before failure. The combination of wear, electrical, and heat resistance makes the refractory metals excellent candidates for the metal used in the integration [12].

The elements that are categorized as refractory metals are tantalum, tungsten, molybdenum, niobium, and rhenium. If the overall category of refractory metals is expanded slightly, elements like titanium, zirconium, and hafnium can be included as refractory metals. All of these metals readily form carbides and silicides, meaning they would be good candidates for researching how the matrix will diffuse and effect the overall properties of the metals in the CMC. The metals that were chosen for this research included tantalum, tungsten, and molybdenum. These metals were chosen because they fit directly into the original definition of refractory metals and they were readily commercially available. They were also chosen for their very high melting temperatures. Tungsten melts at 3380°C, molybdenum melts at 2610°C, and tantalum melts at 3000°C.

These temperatures are well above normal CMC operating temperature [12]. Tantalum is commonly used in the electric industry. Molybdenum is commonly used as an alloying metal to improve overall hardness and corrosion resistance. Tungsten is used as an electrical contact, radiation shields, and targets for x-ray tubes [13].

1.8 Outline of this Thesis

This research is to study the diffusion of Si and C species in a metallic network embedded in a silicon carbide fiber– silicon carbide matrix ceramic composite (CMC) at high temperatures. A fully processed CMC with tungsten, tantalum, and molybdenum wires will be heated at various temperatures for the same duration. The diffusion zone will be measured and then kinetics equations will be applied to determine the failure kinetics.

Chapter 1: Introduction – A brief summary of CMC processes and applications.

Chapter 2: Theory – A brief summary of the diffusion kinetics theory and previously published papers describing various diffusion methods.

Chapter 3: Analysis Methods – Explanations of SEM, EDS, and Raman spectroscopy analysis.

Chapter 4: Processing & Characterization of “Mock” CMCs – The description of the processing of “mock” CMCs and the results seen from the study.

Chapter 5: Processing & Characterization of 1100°C CMC – The description of the processing of the 1100°C CMC and the results seen from the study.

Chapter 6: Si and C Diffusion Study in CMCs at High Temperatures – The analysis of the diffusion silicon and carbon diffusion into CMCs at relevant CMC operating temperatures.

Chapter 7: Summary and Conclusion – The summary of the results seen from the three studies and how they are relevant to CMC processing and applications.

2. Theory

2.1 Carbides and Silicides of Ta, W, and Mo

2.1.1 Phase Diagrams

The tantalum, tungsten, and molybdenum metals were chosen for this study because of their high melting and operating temperatures, electrical resistance, and thermal conductivity. However, this is just looking at the metals in the pure form. There is a high possibility that the metals will react with the system that they are embedded in when trying to examine if it is possible to place refractory wires in a CMC. In this research, the three metals are placed in a SiC/SiC CMC, so it is important to investigate the carbides and silicides that could be potentially formed during CMC processing and operation. In order to investigate the potential silicides and carbides, a literature review was conducted to determine what happens with the metal-carbon systems, metal-silicon systems, and metal-silicon carbide systems at elevated temperatures.

Upon research, a few different papers were found that detail the phase diagrams for silicon and the three different metals. Figure 7 shows the phase diagram between silicon and tantalum. Figure 8 shows the phase diagram between silicon and tungsten, and finally Figure 9 shows the phase diagram for silicon and molybdenum.

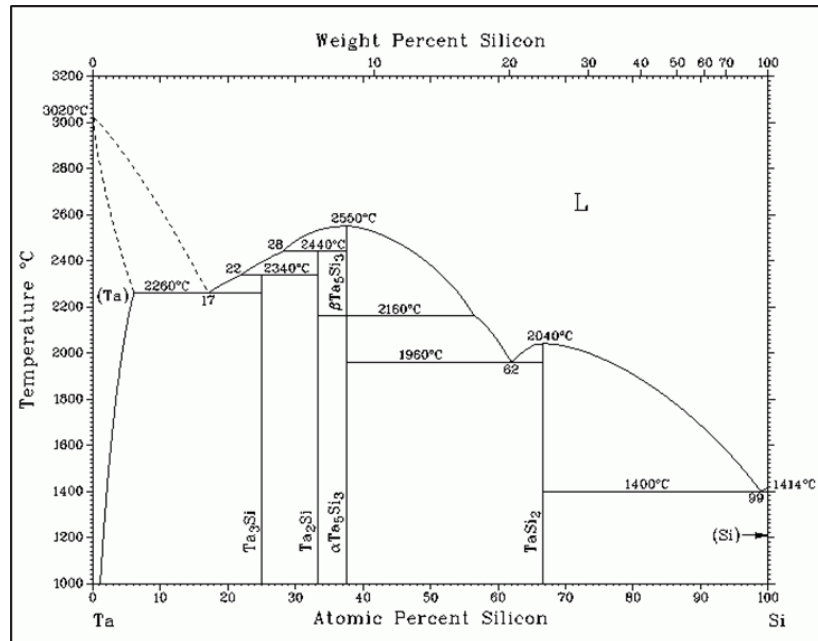


Figure 7: Phase diagram for silicon and tantalum; [14].

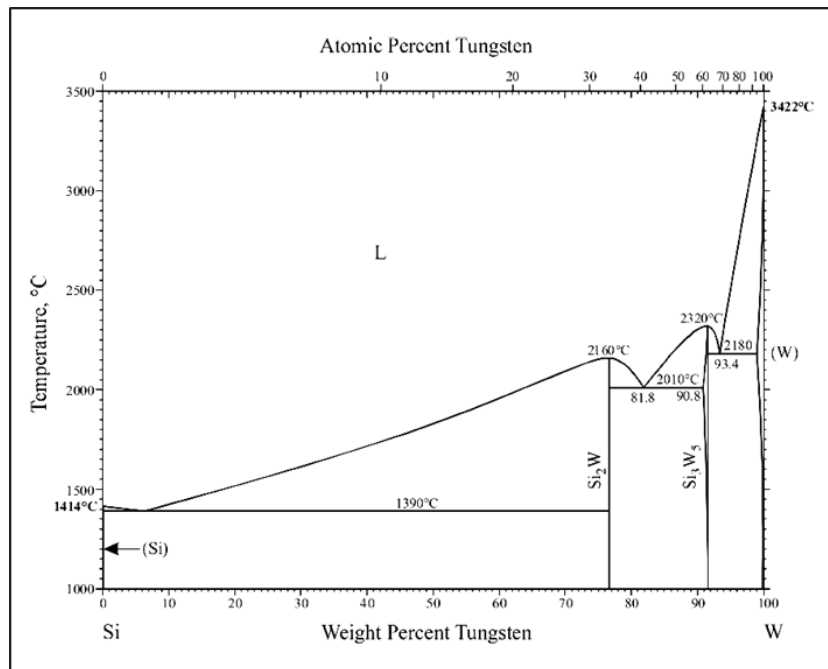


Figure 8: Phase Diagram for silicon and tungsten; [15].

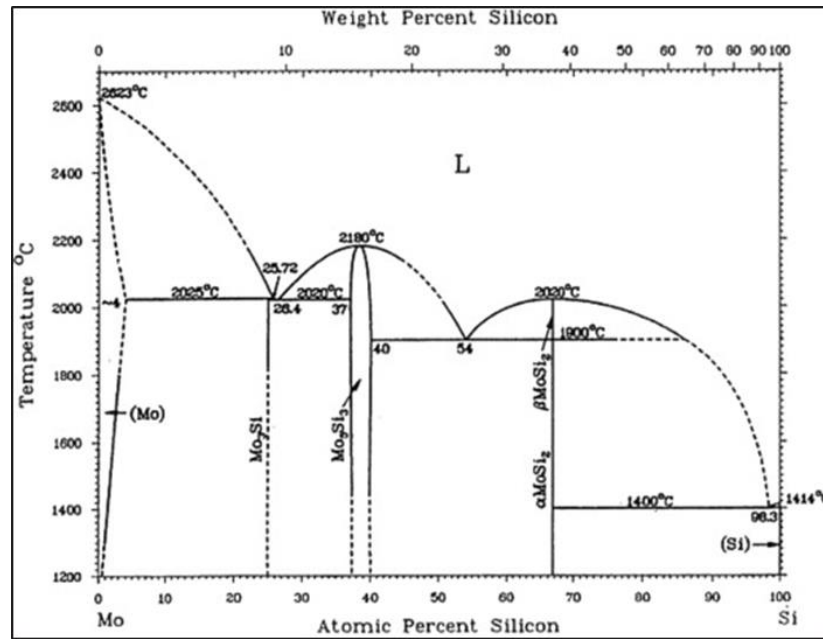


Figure 9: Phase Diagram for silicon and molybdenum; [16].

It can be seen from these three different phase diagrams that silicon and the three refractory metals have very high temperature silicides that are formed. The temperatures at which these silicides are formed are much higher than normal CMC processing temperatures. However, these temperatures are relevant for actual CMC operating temperatures. Upon further research into the different silicides that are formed with each metal, a trend appeared in the crystallographic data. There were two different silicide phases that were present in tantalum, molybdenum, and tungsten. Those phases were 1:2, metal to silicon, and 5:3, metal to silicide. The 5:3 phases all have the space group $I4/mcm$. The 1:2 phases are in all different space groups. $TaSi_2$ has the space group $P6_222$, $MoSi_2$ has the space group $I4/mcm$, and WSi_2 $I4/mmm$ [17]. The common phases indicate that the silicides will all have similar properties.

The carbon phase diagrams, and crystallographic data were found in a similar way.

Figure 10 shows the tantalum carbon phase diagram, Figure 11 shows the tungsten carbon phase diagram, and Figure 12 shows the molybdenum carbon phase diagram.

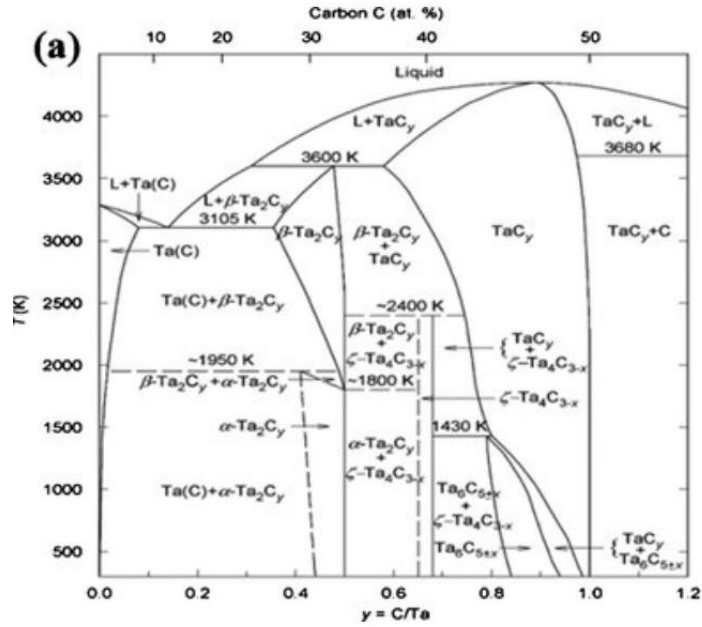


Figure 10: The tantalum carbon phase diagram; [18].

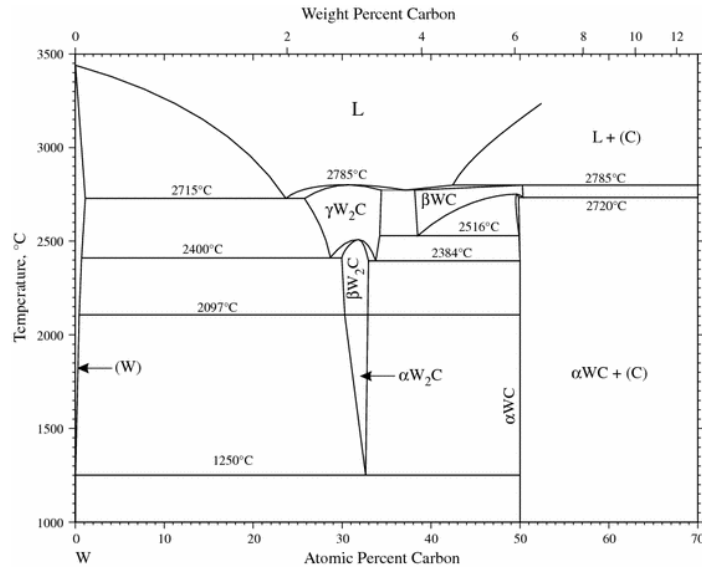


Figure 11: The tungsten carbon phase diagram; [19].

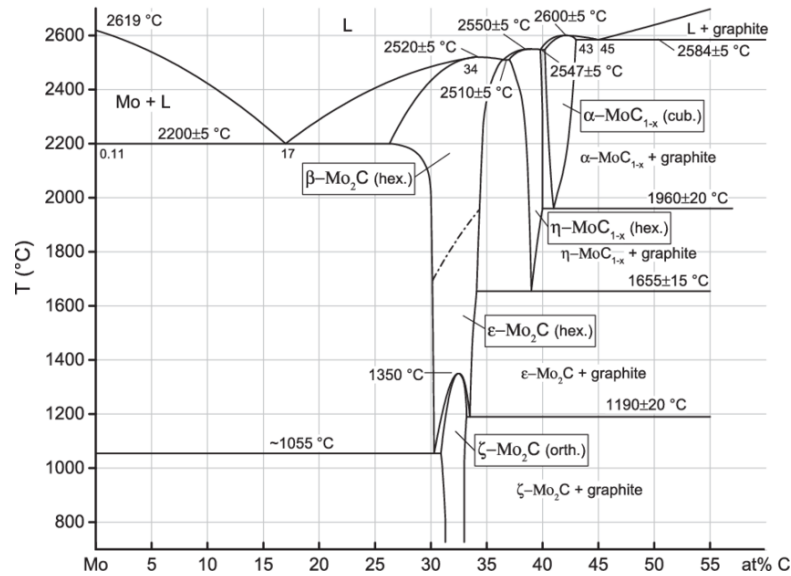


Figure 12: The molybdenum carbon phase diagram; [20].

Similarly, to the silicides seen with the refractory metals, the carbides formed with the refractory metals are at high temperature. There was also a trend noticed in the crystallographic data for the carbides. For all three refractory metals, there was a 2:1, metal:carbon, carbide phase. The space group for W_2C is $P3ml$, the space group for Mo_2C is $P12$, and the space group for Ta_2C is $P3ml$. Tungsten and tantalum also shared another similar carbide phase. The phase is a 1:1, metal:carbon. They both have different space groups. The WC space group is $P6m2$, and the TaC space group is $Fm3m$ [17]. This phase was not seen in the molybdenum carbides.

2.2 Past Experimental Studies

L. Brewer investigated the effects of refractory metals with silicon at temperatures above $1900^{\circ}K$. The known phases of the refractory metal silicides were not known to be stable or high-melting compounds. Only two known metal-silicon phases had a higher melting point than silicon; VSi_2 and $CeSi$, $1927^{\circ}K$ and $1710^{\circ}K$, respectively, as compared to silicon, $1687^{\circ}K$. Brewer's group was motivated to continue investigations with the

metal-silicide phases since there was comparable data and studies involving halides, nitrides, sulfides, carbides, and oxides with the refractory metals showing high-melting compounds.

The experiments conducted by Brewer involved direct synthesis of the metal silicides. The metals investigated were tungsten, tantalum, and molybdenum. The metal purity was confirmed by X-ray diffraction and the silicon purity was 99.87%, the impurities were carbon and aluminum. The metals and silicon were mixed together in 100 to 400 mesh powders and heated in an induction furnace to various temperatures above 1900°K. The length of the heating was three minutes, but the samples were reheated at a higher temperature if equilibrium was not reached during the initial three minutes. The atmosphere was about three fourths argon in order to prevent the volatilization of silicon during the reactions. The crucibles used were non-degassed silica and the weight of the crucibles and powders were measured before and after heating. The weight loss was assumed to be silicon volatilization and around a 1% weight change was recorded. The ratios of the refractory metals to silicon were then calculated.

There were three tantalum silicide phases formed. The phase known due to prior research was TaSi₂. These phases were found via X-ray diffraction studies. The known TaSi₂ phase displayed a gradually weaker signal as the atomic percentage of silicon decreased from 65 to 38%. The newly identified phase, TaSi_{0.60}, became stronger as the atomic percentage of silicon decreased. The tantalum silicide sample with 43% silicon gave a stronger TaSi₂ and a weaker TaSi_{0.60} signal. At 38 atomic percent silicon, the TaSi₂ phase was no longer observed and the only signal was from the TaSi_{0.60} phase. Further

reduction of the atomic percentage of silicon showed another new phase, $\text{TaSi}_{0.40}$, which was observed at 37, 36, and 33 atomic percent silicon.

The reaction of molybdenum and silicon formed three phases, only one of which had been previously reported, MoSi_2 . The new phase found, $\text{MoSi}_{0.65}$, increased in signal intensity from 65 to 40 atomic percent silicon and from 24 to 40 atomic percent silicon. At 40 atomic percent, only the phase $\text{MoSi}_{0.65}$ was reported. While the $\text{MoSi}_{0.65}$ phase was increasing, the previously reported phase, MoSi_2 , and the other new phase found, Mo_3Si , were decreasing in signal intensity.

The tungsten and silicon studies found one new phase that had not been previously report, $\text{WSi}_{0.7}$. The phase that had been reported prior to this study was WSi_2 . The new phase was only reported at 41 atomic percent of silicon. At higher atomic percentages of silicon, there were mixtures with WSi_2 . At lower atomic percentages of silicon, there were mixtures with tungsten. The location of the $\text{WSi}_{0.7}$ did not change at the different atomic percentage of silicon [21].

Brewer's theory that refractory metal silicides, specifically molybdenum, tungsten, and tantalum, would be high-melting is verified by the experiment described above. This study also resulted in the identification of two new tantalum phases, two new molybdenum phases, and one new tungsten phase. This study is relevant to this thesis because it heats the refractory metals with silicon at temperature comparable to CMC processing without added pressure. While this study focused on powdered silicon and metals and did not include carbon, the temperature is similar to the higher temperature range for CMC processing.

Brewer continued to investigate the silicides of various refractory metals, specifically, tantalum, molybdenum, and tungsten, to determine their thermodynamic stabilities. The thermodynamic stabilities of the refractory silicides directly correlate to how importance and usefulness of the phases. The heats of formation are of thermodynamic importance; however, the typical combustion calorimetry and solution calorimetry methods are not applicable for silicides. Silicides have an inertness towards oxidation reactions and solvents. Due to this, the method of dissociation pressure measurements is the best way to determine the refractory silicide's thermodynamic stabilities. Equilibrium studies conducted by Brewer consisted of M-Si, M_1 - M_2 -Si, M-Si-C, and M-Si-N₂. The two systems of interest to this thesis are M-Si and M-Si-C. The M-Si system is a continuation of Brewer's work from 1950 and the M-Si-C system is directly comparable to the SiC/SiC CMC with the metal embedded in the matrix.

The experimental procedure Brewer followed for the metal silicide interactions involved mixing together 140-400 mesh powders and heating them to 2100°K for any time between 15-60 minutes. The starting materials for the eventual powder mixture were silicon metal ground into a fine mesh, less than 140, using a mortar and pestle. Analysis was done to the silicon powder to determine the impurities present. It was found that the impurities were we Al with 0.1%, Fe with 0.1%, Ti with less than 1%, and Cr with 0.1-1%. All of the refractory metals obtained were of 99.9% purity or higher. This heating was done in 0.75 atmospheric argon to prevent silicon volatilization. After the heating, x-ray diffraction analysis, XRD, was done to determine what phases were present.

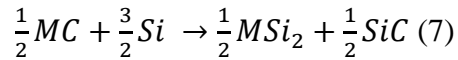
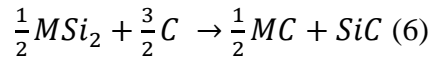
Brewer found two new tantalum silicide phases, TaSi₂ and Ta₅Si₃. There was a new phase found for both tungsten and molybdenum, WSi₂ and MoSi₂. The other phases that were

reported by Brewer were seen and previously identified in his previous paper, High Melting Silicides, which was published in 1950 and referenced above.

The M-Si-C system was determined through various calculations. Brewer determined that the limitations on the heats of formation of the silicides are based on the heats of formation of the carbides. Brewer utilized Equation 5, assuming that ΔS°_{298} was zero when all of the reactants, carbides, silicides, and metals, were solids.

$$\Delta F^\circ_T = \Delta H^\circ_{298} - T\Delta S^\circ_{298} \quad (5)$$

An example of the calculations done by Brewer can be seen in Equations 6 and 7. The ΔH°_{298} was known for silicon carbide and the metal carbide, so the ΔH°_{298} of the metal silicide could be determined.



By utilizing the heats of formation calculations, Brewer was able to determine ternary phase diagrams for the M-Si-C systems. Figure 13 shows the ternary phase diagram for Mo-Si-C. Figure 14 shows the ternary phase diagram for Ta-Si-C and Figure 15 shows the ternary phase diagram for W-Si-C. The common phases between each of the three metals are circled in red [22]

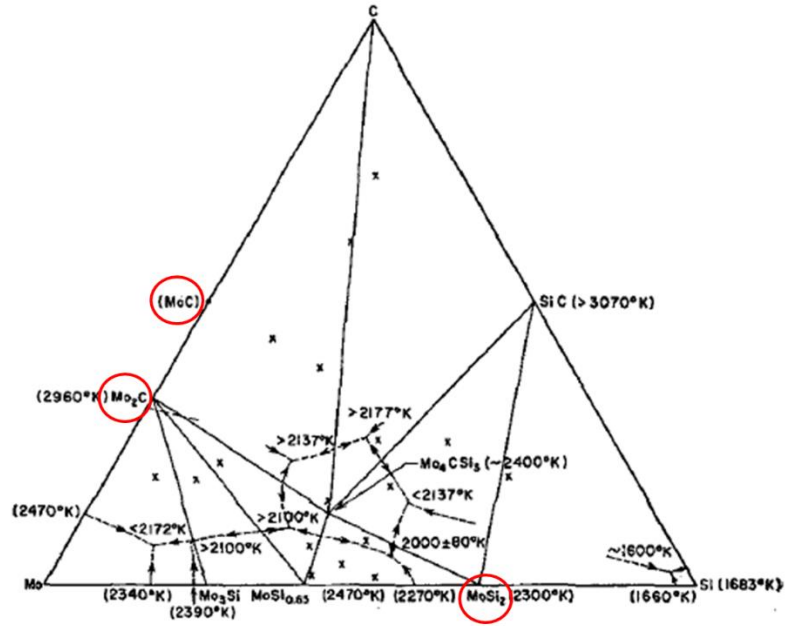


FIG. 6. Mo-Si-C system

Figure 13: The Mo-Si-C system ternary phase diagram as determined by Brewer in 1956; [22].

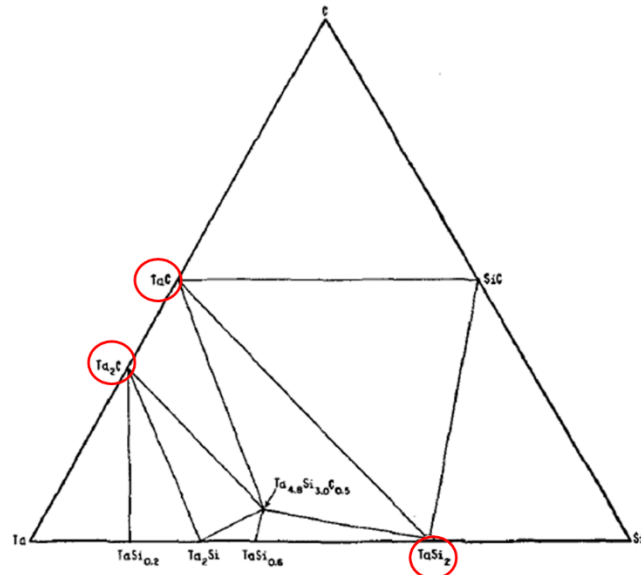


FIG. 5. Ta-Si-C system

Figure 14: The Ta-Si-C system ternary phase diagram as determined by Brewer in 1956; [22].

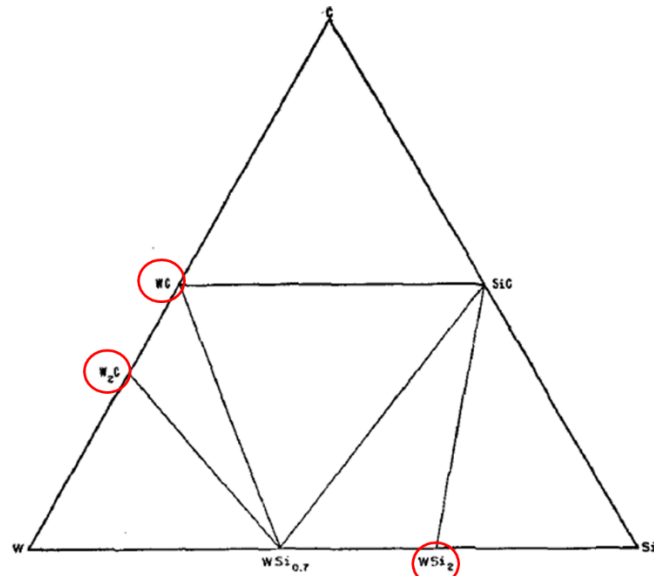


FIG. 7. W-Si-C system

Figure 15: The W-Si-C system ternary phase diagram as determined by Brewer in 1956; [22].

This work by Brewer helped to define new silicide phases and determine the M-Si-C system ternary phase diagrams. The relevance to this thesis is that it directly involved the three systems of interest, Mo-Si-C, Ta-Si-C, and W-Si-C. This study is not completely relevant to this thesis, however. While it does include the three metals of interest, the metals utilized in this experiment were powders, and not wires as utilized in this thesis. The temperature processed at were much higher than the temperature used in this thesis. However, this was very informative to see how the metals interact with silicon in carbon.

The next paper investigated for this thesis was by B.V. Cockeram and involved the diffusion bonding of silicon carbide with refractory metals. The research was conducted to determine the bond quality between different refractory metals foils with plates of silicon carbide. Cockeram used both α -SiC and β -SiC.

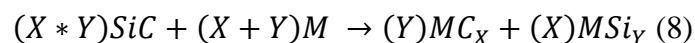
Cockeram used Hexology™ SA SiC (Carborundum Co), a single phase, sintered α -SiC, plate that was lapped to a smooth finish. The β -SiC that was used was CVD SiC (Morton

Advanced Materials). It was also a single phase and lapped to a smooth finish. Metal foils were obtained from Alfa Aesar. This study only investigated tungsten and molybdenum, excluding tantalum. The foils obtained were molybdenum 12.7 μm and 25.4 μm , both at 99.9% purity, and tungsten 50.8 μm at 99.95% purity. The metal foils were placed in direct contact with the silicon carbide plates. A weight was applied to apply a specific pressure. The sample was then heated. Different bonding temperatures and bonding pressures were used along with the different foil thicknesses. The weight applied resulted in a range of 3.4 MPa to 18.6 MPa applied to the system. The samples were heated at a rate of 500°C/hour to 300°C/hour to a final temperature of 1200°C to 1500°C. This was then held at temperature for 10 hours and cooled. Figure 16 shows the different experiments done to the metal foils of interest to this thesis.

7	Mo (12.7 μm)	CVD SiC	0.89 X 0.89 X 0.25	1200	10	3.4	No Bonding.	---
8	Mo (12.7 μm)	CVD SiC	0.89 X 0.89 X 0.25	1500	10	3.4	Bonding. Good Quality.	1.6
9	Mo (12.7 μm)	H-SA SiC	1.27 X 1.27 X 0.32	1500	10	8.8	Bonding. Good Quality.	---
10	Mo (12.7 μm)	H-SA SiC	1.27 X 0.64 X 0.32	1500	10	17.2	Bonding. Good Quality.	---
11	Mo (12.7 μm)	CVD SiC	1.27 X 1.27 X 0.36	1500	10	8.8	Bonding. Good Quality.	---
12	Mo (12.7 μm)	CVD SiC	1.27 X 1.27 X 0.36	1500	10	8.8	Bonding. Good Quality.	---
13	Mo (25.4 μm)	CVD SiC	1.27 X 0.64 X 0.36	1500	10	17.2	Bonding. Fair Quality.	---
14	W (25.4 μm)	H-SA SiC	1.27 X 0.64 X 0.32	1500	10	17.2	Bonding. Fair Quality.	1.4

Figure 16: The metal foils, type of silicon carbide, final temperature, applied pressure, and overall bond quality of the relevant studies in Cockeram's research; [23].

Cockeram found that the refractory metal carbides are more stable than silicon carbide when compared thermodynamically. It was stated that direct contact between the silicon carbide and the metal carbide would result in a full conversion following Equation 8.



The type of analysis that was used to determine the overall bond quality was SEM, microprobe, and AES. When analyzing the SiC/Mo/SiC bonds, Cockeram reports that higher temperature was needed to produce strong bonds for both CVD SiC and Hexology™ SA SiC. There was a low density of cracks observed in the bond region and the increase in pressure did not result in an increase in overall bond quality. It was noted that the thicker the bond foil was, the higher density of cracks was observed. Molybdenum and silicon carbide have similar coefficients of thermal expansion, so Cockeram theorizes this was the reason for the high bonding quality observed in the SiC/Mo/SiC system. Figure 17 shows the CVD SiC plates in contact with the molybdenum foil and has arrows pointing to the different phases formed during the reaction.

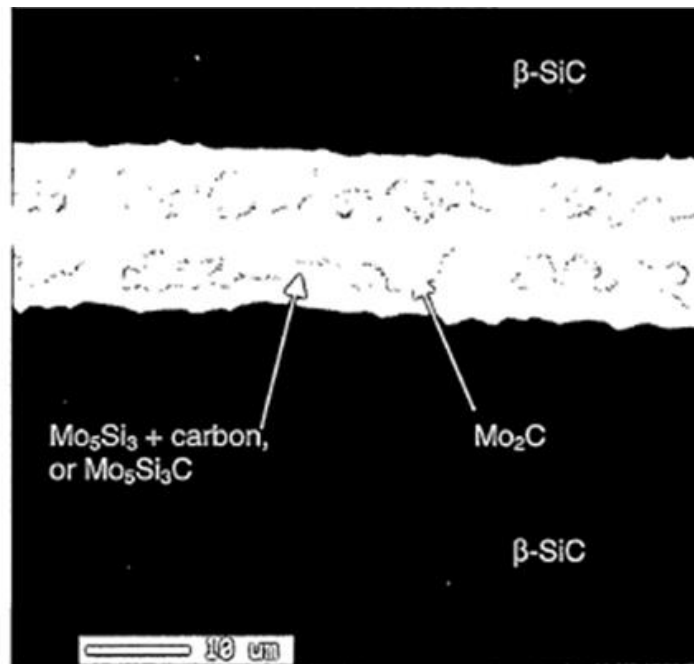


Figure 17: The SiC/Mo/SiC system after heating; [23].

Upon analyzing the SiC/W/SiC bonds, Cockeram reported that there was a higher density of cracks observed than in the SiC/Mo/SiC system. It is theorized that this is due to the

thicker foil used in the tungsten system and the greater difference in the coefficient of thermal expansion for tungsten and silicon carbide. There was a complete conversion of the materials to tungsten carbides and tungsten silicides. The diffusion path $\text{SiC} \rightarrow \text{WC} \rightarrow \text{W}_5\text{Si}_3 \rightarrow \text{W}_2\text{C} \rightarrow \text{W}$ was determined. Figure 18 shows the diffusion path in the SiC/W/SiC system. Figure 19 shows the diffusion path applied to the tungsten ternary phase diagram with silicon and carbon. The common phases seen in the silicides and carbides for all three metals are circled in red.

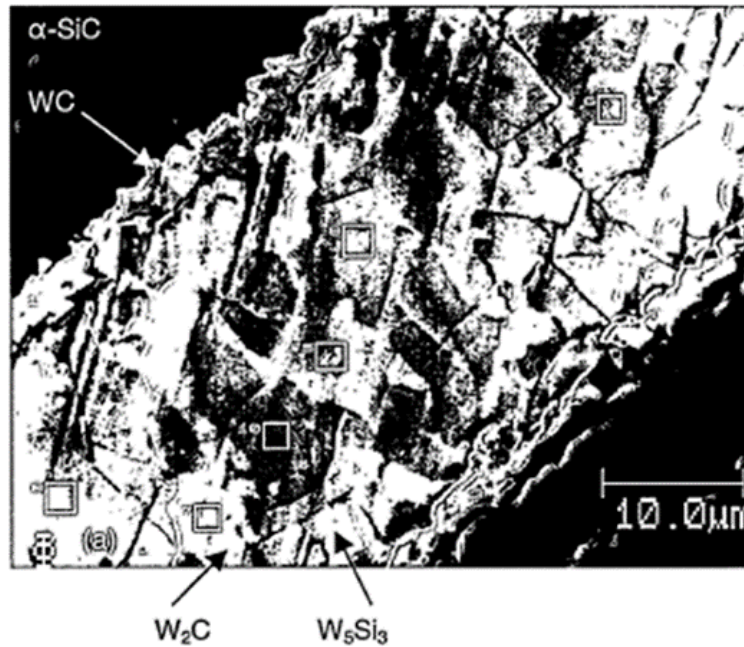


Figure 18: The tungsten diffusion path in the SiC/W/SiC system; [23].

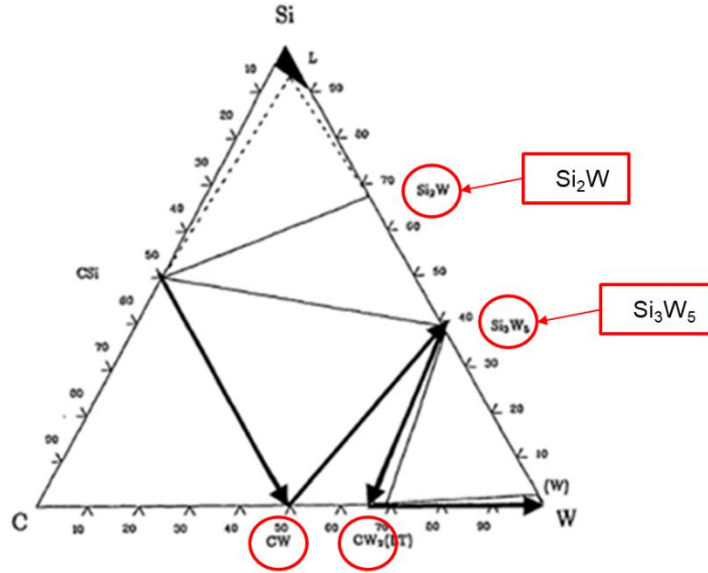


Figure 19: The diffusion path overlayed on the W-Si-C ternary phase diagram; [23].

Overall, Cockeram determined that the formation of cracks was due to the volume change from the differences in coefficients of thermal expansion and the formation of silicides and carbides during the heating of the metal foils and the silicon carbide plates. The applied pressure had no influence on the overall bond quality and the thinner foils resulted in a lower density of cracks around the bonding region [23].

Cockeram's research is very relevant to this thesis as it used solid silicon carbide and refractory metals. The processing temperature is also very similar to that of CMC processing temperatures. It also analyzed silicon carbide in direct contact with molybdenum and tungsten. However, it does differ from the research conducted for this thesis because it used metal foils instead of wires and plates for the silicon carbide instead of fiber weaves and slurry. It also added pressure to the system, but it did not result in better bonding quality, so that shows that the phases formed during CMC processing does not have to rely on added pressure, thus deviating from the normal CMC processing parameters.

These papers helped determine the potential phases that could be seen after CMC processing with the refractory metals embedded in a SiC/SiC CMC. There were major differences in every paper though that does not allow them to be directly applicable to this thesis research. None of these papers, or other ones found, had a system similar enough to the one being tested in this research, thus verifying the novelty of conducting this research. The study of the placing the metal wires in between fiber weaves in the layup, as further described later in the paper, will result in interesting diffusion phenomenon that has not been recorded anywhere else.

2.3. Diffusion

2.3.1. Arrhenius Equation

The diffusion zones seen in the refractory metals after different CMC processing temperatures, as further detailed and described later in the paper, need to be identified. Normally, x-ray diffraction analysis would be used to determine the phases formed, but the size of the diffusion zone was too small for it to be determined. Because of that, different routes had to be taken to analyze the diffusion phases formed within the wires.

By using the Arrhenius equation, the activation energy and the diffusion coefficient can be determined. The Arrhenius equation is a relationship between the temperature of a reaction and the rate at which it occurs. Equation 9 shows the Arrhenius equation. K is the diffusion rate coefficient or the parabolic coefficient. K_0 is the diffusion constant or pre-exponential factor. Q is the activation energy, R is the gas constant, and T is the processing temperature.

$$K = K_0 e^{\frac{-Q}{RT}} \quad (9)$$

This equation can be utilized to determine the activation energy and the diffusion constant [24]. Another equation is needed to determine the diffusion rate coefficient, K . That equation and its application is described below.

2.3.1. Experimental Example

Yang conducted an experiment that detailed the diffusion rate coefficient derivation by utilizing an isothermal heat treatment and then applied it to the Arrhenius equation to determine the activation energy. The purpose of Yang's research was to determine the diffusion rate, K , from atomic diffusion in spark plasma sintering, SPS.

The system used by Yang was CuTi and Cu₄Ti. The materials were received as ingots and then they were hot rolled, and vacuum annealed to ensure fine grain size. This also allowed for the elimination of any residual stresses from hot rolling. The annealed samples were then formed into rods. The end surfaces of each rod were machined to be parallel and polished to a fine surface. The rod ends were placed in direct contact with each other and rolled in graphite foil to ensure the pulsed electric current, PEC, generated from the SPS, passed directly through. There were four different heating rates used: 600°C for 20 minutes with a PEC intensity of 500 A, 650°C for 40 minutes with a PEC intensity of 560 A, 700°C for 60 minutes with a PEC intensity of 620 A, and finally 750°C for 80 minutes with a PEC intensity of 680 A. After the heating was done to the samples, they were sectioned axially and polished to a fine finish. The thickness of each reaction was then measured with an SEM and EDS detector.

Yang determined that the growth process seen in the two systems can be considered a diffusion controlled process. Because of this, it represents a parabolic-type relation as

seen in Equation 10. K represents the diffusion rate coefficient, x is the thickness of the formed diffusion zone, and t is the isothermal time spent at the temperature.

$$K = \frac{x^2}{t} \quad (10)$$

After the diffusion rate coefficient was determined, it was directly applied into the Arrhenius equation and the activation energy and diffusion constant was determined for each system [24].

This is very relevant to this research because it takes a diffusion controlled process and uses the Arrhenius equation to determine the activation energy and diffusion constant. The methodology in determining the diffusion rate coefficient is within the scope of this research. The diffusion zone thickness can be measured and then the time spent at the final temperature can be applied to determine the diffusion rate coefficient. This can then be used in the Arrhenius equation, with the final processing temperature added in, to determine the activation energy and diffusion constant. The application of this process is described in full detail later in this paper.

3. Analysis Methods

3.1 Scanning Electron Microscopy

Scanning electron microscopy is useful in showing features that are very small and cannot be seen with the naked eye. The scanning electron microscope, SEM, consists of a source of high energy electrons and a condenser system. A probe lens is used to focus the beam of high energy electrons and directs it at the sample. When the beam comes in contact with the surface of the sample, it interacts with the sample and results in six potential outcomes for the electron beam. The potential outcomes are secondary electrons, backscattered electrons, x-ray (energy dispersive/wave dispersive), Auger electrons, cathodoluminescence, and transmitted electrons. This can be seen in Figure 20.

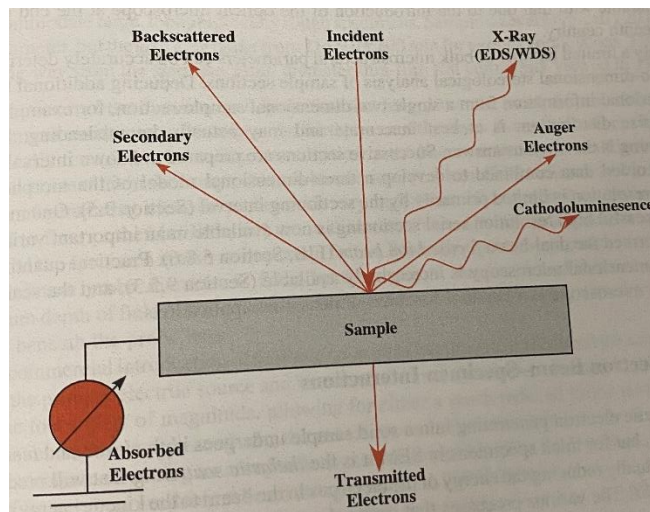


Figure 20: The potential interactions after the incident electrons hit the surface of the sample; [25]

There are detectors built into the SEM to collect the different signals coming off of the sample after the electron beam interacts with the surface of the sample. The most common detectors include are secondary electron, SE, detectors, and backscattered electron, BSE, detectors. These two detectors generate an image of the surface of the sample. There are different parameters that can be changed to enhance the image formed, such as the working distance, the aperture, and the beam voltage [25].

The SEM that was used in this thesis was the Zeiss Gemini SEM 500. The detector that was utilized in this study was the SE detector. The Gemini SEM is very useful for imaging features on the nano-size scale but has its limitation with imaging of large features. When the magnification of the microscope is at the lowest, around 150x, there is slight warpage around the edges. To image the entire size of the wires embedded in the CMC, the magnification was pulled all the way out, resulting in slight image distortion. However, when the magnification was increased, the warpage disappeared, and the images were clear. The other major detector that was used was the EDS detector, which detect x-ray signals that are from the surface of the sample.

3.2 Energy Dispersive Spectroscopy

Energy dispersive spectroscopy, EDS, is another detector that is in the Gemini SEM. EDS detectors collect the photons that escape from the surface of the material due to excitation from the electron beam. The detectors collect the photons and interpret them as a function of the energies they possess. This is then used to determine the chemical composition of the sample. This is very useful to determine what elements are present within a sample, how different atoms diffuse over time, and different compositional gradients present. The EDS detectors are highly efficient and can collect the excited

photons over a wide range of the sample. However, there are limitations associated with the detection. Characterizing the specific elements is dependent on the characteristic peaks from the x-ray signal generated from each element. There are many areas where these peaks overlap from element to element, resulting in inaccurate data [25]. The peak overlap phenomenon occurs during this experimental study and will be fully discussed later in this paper.

3.3 Raman Spectroscopy

Raman spectroscopy is based on the theory of Raman phenomenon. Raman phenomenon is the inelastic scattering of light by matter. When this occurs, there are two different types of scattering behavior; one involves no energy transfer, and one involves an energy transfer. The scattering behavior that results in no energy transfer between the light and the sample is elastic and is referred to as Rayleigh scattering. The scattering that involves an energy transfer is inelastic and is referred to as Raman scattering. The energy transfer results in a scattered photon that has a new energy that is equal to the sum of the natural frequencies of the sample and the frequencies of the incident photon.

A Raman instrument will consist of a laser, which acts as the excitation light source, a guiding system, a spectrometer, a detector, a data acquisition unit, and an optical microscope to allow for the sample to be seen. The laser source utilized for this study was a 633 nm laser. The spectrometer's use in the system is to separate the Rayleigh scattering signal from the Raman scattering signal. The spectrometer also analyzes the collected signals and sends the proper information to the detectors. The data acquisition software is used to analyze the received signals [26].

Raman spectroscopy was utilized in this experiment to map the carbon content in each sample and to map the carbon content migration towards the wire after different heating cycles were applied. Further explanation of the specific collection and analysis parameters are explained fully later in this paper.

4. Processing and Characterizations of “Mock” CMCs

In order to functionalize a CMC with integrated metallic substrate of a comparable feature size, information about how the refractory metals react during the CMC processing is necessary. The refractory metals, tungsten, tantalum, and molybdenum readily form silicides and carbides. Documentation of the phases formed and at what temperatures is necessary before forward progress can be made to functionalize the CMC. Before the phases are analyzed, an important step is making sure that the metals actually survive the CMC processing. The processing of a CMC is done at elevated temperatures and repeated cyclically. To determine if the metals survived the processing, the refractory metals were purchased in two different gauged wires, 250 microns and 500 microns. “Mock” CMCs were then created. The term mock is applied to these samples since they are not fully processed CMCs. The CMCs were made without the stacking of fiber weaves. The “mock” CMCs consisted of SiC powder and SMP-10 slurry. The fiber weaves are extremely expensive to purchase, difficult to process and cut, and add a significant amount of time to the layup process. The reactions that will occur within the wires will be due to the SiC and SMP-10 slurry, not from the fiber weaves, so they were excluded for this initial test. There were three separate “mock” CMCs processed at different CMC processing temperatures.

The objective of doing this initial test was to see how common CMC processing temperatures affect the metals during the cyclical heating and if the metal wires survived the processing.

4.1 Experimental Aspects

4.1.1 Layup

The layup process for making the “mock” CMCs varied slightly from the generalized CMC layup process that was described previously. The typical CMC layup process involves coating ceramic fiber weaves in a ceramic powder and pre-ceramic polymer slurry mixture. For the “mock” CMC, the fiber weave was left out of the layup. The main constituents that will potentially form carbides and silicides with the refractory metals are the ceramic powder and pre-ceramic polymer.

A metal plate was outlined with two different types of tape that were used to seal the bagging material to the plate and around the composite. The tapes were AVBS 759 and A-800-3G (Airtech Advanced Materials Group, Huntington Beach, CA). These specific tapes were chosen because the maximum operating temperature is 400°C and 427°C, respectively. On the inside of the tape outline, Teflon was taped down to the plate to prevent any of the excess slurry was curing on the plate. The tape that was used a polyimide pressure sensitive tape, Airkap 1 (Airtech Advanced Materials Group, Huntington Beach, CA). Airkap 1 was chosen due to its maximum operating temperature of 399°C. Once this plate was prepared, the creation of the “mock” CMC began.

The refractory metal wires were purchased in two different gauge sized, 250 microns and 500 microns. The tantalum wires are 99.9% purity, the tungsten wires are 99.95% purity, and the molybdenum wires are 99.95% purity (Goodfellow Cambridge Limited,

Huntingdon PE29 63R England). The wires were shipped on a spool, so the wires were slightly curved. This made it difficult to control the placement of the wires, so they were straightened out by hand. The 250 micron wires were made into one composite and the 500 micron wires were made into another. The wires were spaced so that they were not touching each other to prevent metal to metal interaction.

The slurry was 35 volume percent. It consisted of 7-micron SiC powder (99.5%; Materion Advanced Chemicals, Milwaukee, WI) and the pre-ceramic polymer (StarPCS™ SMP-10; Starfire Systems, Inc. Schenectady, NY). The slurry was mixed together in a planetary mixer (ARV-310, THINKY, Laguna Hills, CA) to ensure that it was thoroughly mixed together and homogenous.

Figure 21 shows the layup process of the slurry and wires. The wires were placed within the slurry. Once this was finished, the preparation for the “mock” CMC to go into the autoclave (EC-2X4-200P800F2S2P4T; ASC Process Systems, Chatsworth, CA) began.

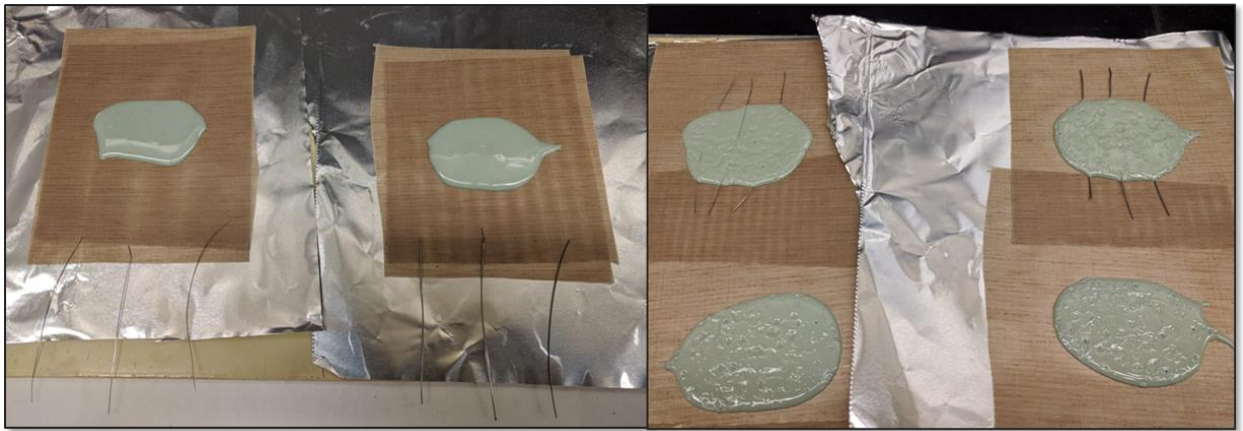


Figure 21: The “mock” CMC layup process.

A smaller metal plate was covered with Teflon and taped down with the Airkap 1 tape.

This was then placed on top of the “mock” CMC resting on the bigger metal plate. This

second plate acted as a weight to ensure that the composite stayed together and did not shift during processing. The edges of the second plate were covered with fiberglass (8.9oz Fiberglass E Cloth; US Composites, Inc., West Palm Beach, FL) to prevent the corners from ripping the vacuum bag. The plate and fiberglass were then taped down to the bigger plate with Airkap 1 to prevent any movement when vacuum was pulled. Figure 22 shows the weighted plated resting on the “mock” CMCs.

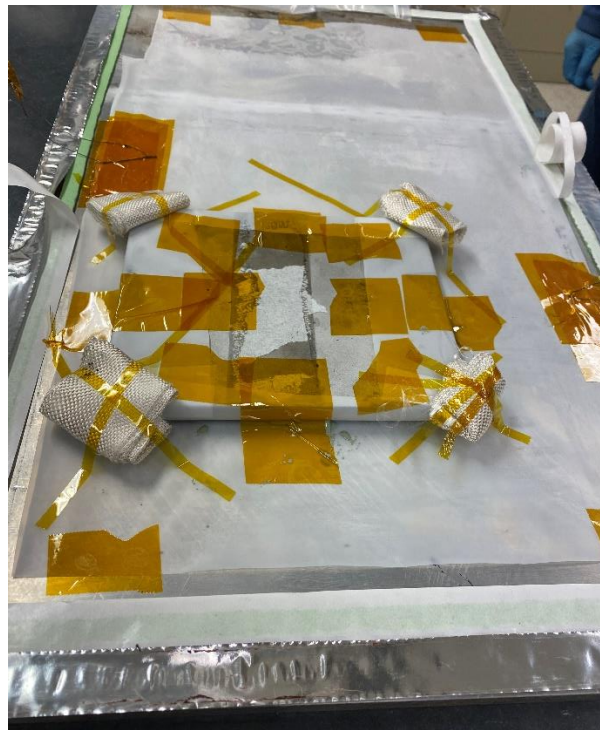


Figure 22: The weighted plate resting on the “mock” CMC to prevent movement when the vacuum is pulled.

Thermocouples were then attached to the plate with the Airkap 1 tape so the temperature of the composite could be recording during the autoclave processing. Extra fiberglass cloth was placed around the entire metal sheet as a breather cloth to ensure that the vacuum bag did not catch or tear on anything during processing. A puncher was used to put holes into the bagging material (Thermalide; Airtech Advanced Materials Group, Huntington Beach, CA) for the vacuum ports (Vac Valve 409 SSHTR; Airtech Advanced

Materials Group, Huntington Beach, CA) to go through. The bagging film with the vacuum ports was then placed over the larger metal plate. The protective coverings on the AVBS 759 and A-800-3G tapes were removed and the film was pressed into them, ensuring a good seal and no gaps or kinks. The thermocouples were left out of the bag so the connector sites could be placed properly in the autoclave. The vacuum hoses (Airflow 800; Airtech Advanced Materials Group, Huntington Beach, CA) were then attached to the vacuum ports. The plate was loaded into the autoclave and the vacuum hose and thermocouples were connected. Figures 23 and 24 show the vacuum ports connected to the plate and the plate loaded into the autoclave. The autoclave applied 100 psi of pressure. The process parameters can be seen in Table 1.



Figure 23: The fully vacuumed bagged plate with the thermocouple and vacuum ports attached to the plate.



Figure 24: The plate loaded into the autoclave with the thermocouples attached, the vacuum hoses attached, and the vacuum pulled.

Table 1: The autoclave processing parameters for the “mock” CMCs.

Autoclave Processing Parameters			
Initial Temperature	RT	120°C	250°C
Final Temperature	120°C	250°C	RT
Heating Rate	10°C/min	10°C/min	10°C/min
Hold Time	1 hour	1 hour	None

After the autoclave run, the layup for the “mock” CMC was finished. This process was repeated two different times for each the 250 micron wires and the 500 micron wires, for a total of four samples. The reasoning was to create two different “mock” CMCs, with identical layup parameters, to be processed at different temperatures.

4.4.2 Processing of Refractory Wires and “Mock” CMC

The first round of testing that was done was to process the refractory wires without putting them in a matrix or creating a “mock” CMC. This was done to see how

the wires would react at the elevated temperature without wasting any silicon carbide powder or SMP-10. The temperature chosen was 900°C. This temperature was chosen because it is the lowest common CMC processing temperature, so it was important to ensure that the wires could at least survive the lowest potential temperature. The wires went through five iterative graphite furnace cycles, replicating CMC processing without the reinfiltration step in between the furnace runs. Table 2 shows the iterative processing parameters for the wires heated without being embedded in a silicon carbide matrix.

Table 2: The iterative pyrolysis processing parameters for the 900°C processed wires.

Iterative 900°C Processed Wires - Graphite Furnace Processing Parameters				
Initial Temperature	RT	320°C	600°C	900°C
Final Temperature	320°C	600°C	900°C	RT
Heating Rate	10°C/min	5°C/min	10°C/min	25°C/min
Hold Time	1 hour	1 hour	1 hour	None

The processing of the “mock” CMC consisted of various reinfiltration cycles, vacuum oven (DZF-6050-HT/500; MTI Corporation, Richmond, CA) run, and graphite furnace (F-14X14X14-GG-2500-VM-G; Materials Research Furnaces, Inc., Allenstown, NH) runs. The first pyrolysis of the “mock” CMCs was to officially turn the cured SiC slurry into a ceramic piece. There were two different final processing temperatures, 1100°C and 1300°C. Tables 3 and 4 show the processing parameters for each final processing temperature.

Table 3: The 1st pyrolysis processing parameters for the 1100°C “mock” CMCs.

1st Cycle 1100°C CMC Graphite Furnace Processing Parameters					
Initial Temperature	RT	250°C	320°C	600°C	1100°C
Final Temperature	250°C	320°C	600°C	1100°C	RT
Heating Rate	10°C/min	10°C/min	5°C/min	10°C/min	25°C/min
Hold Time	None	1 hour	1 hour	1 hour	None

Table 4: The 1st pyrolysis processing parameters for the 1300°C “mock” CMCs.

1st Cycle 1300°C CMC Graphite Furnace Processing Parameters					
Initial Temperature	RT	250°C	320°C	600°C	1300°C
Final Temperature	250°C	320°C	600°C	1300°C	RT
Heating Rate	10°C/min	10°C/min	5°C/min	10°C/min	25°C/min
Hold Time	None	1 hour	1 hour	1 hour	None

After this initial pyrolysis run, the “mock” CMCs were reinfiltrated with the same pre-ceramic polymer, SMP-10, that was used in the slurry and creation of the composite. This was done in two different vacuum chambers. The SMP-10 was placed in one petri dish and the composite was placed in another, each in a separate vacuum chamber. After sitting under vacuum for about one to two hours, a needle and tube were inserted into SMP-10 with the receiving end going into the vacuum chamber with the composite. The SMP-10 transferred from its own vacuum chamber to the vacuum chamber with the composite due to the pressure difference. The SMP-10 and composite were left under vacuum for about one to two hours. After this was completed, the composite was placed in a vacuum oven for the SMP-10 to cure in the pores of the “mock” CMC. The vacuum oven processing parameters can be seen in Table 5.

Table 5: The iterative processing parameters for the vacuum oven.

Iterative CMC Vacuum Oven Processing Parameters				
Initial Temperature	RT	120°C	250°C	320°C
Final Temperature	120°C	250°C	320°C	RT
Heating Rate	10°C/min	5°C/min	5°C/min	5°C/min
Hold Time	1 hour	1 hour	1 hour	None

After the vacuum oven curing, the composite was placed in the graphite furnace to pyrolyze the SiC. Tables 6 and 7 show the iterative graphite furnace pyrolysis cycles that the different “mock” CMCs were processed at.

Table 6: The iterative pyrolysis processing parameters for the 1100°C “mock” CMCs.

Iterative 1100°C Pyrolysis CMC Graphite Furnace Processing Parameters				
Initial Temperature	RT	320°C	600°C	1100°C
Final Temperature	320°C	600°C	1100°C	RT
Heating Rate	10°C/min	5°C/min	10°C/min	25°C/min
Hold Time	1 hour	1 hour	1 hour	None

Table 7: The iterative pyrolysis processing parameters for the 1300°C “mock” CMCs.

Iterative 1300°C Pyrolysis CMC Graphite Furnace Processing Parameters				
Initial Temperature	RT	320°C	600°C	1300°C
Final Temperature	320°C	600°C	1300°C	RT
Heating Rate	10°C/min	5°C/min	10°C/min	25°C/min
Hold Time	1 hour	1 hour	1 hour	None

After the graphite furnace run, the composites were reinfiltrated again. This process was repeated five times for both of the “mock” CMCs. The only difference was the final

processing temperature for each composite. One went to 1100°C and one went to 1300°C. The 1300°C 250 micron composite was then also taken further to 1500°C in the graphite furnace and was held at that temperature for three hours. The 1300°C 500 micron composite was also taken further to 1700°C in the graphite furnace for two hours. Tables 8 and 9 show the additional processing parameters for the 1300°C 250 micron composite and the 1300°C 500 micron composite.

Table 8: The additional pyrolysis processing parameters for the 1300°C 250 micron “mock” CMCs.

Additional 1500°C Graphite Furnace Processing Parameters				
1300°C 250 micron "mock" CMC				
Initial Temperature	RT	320°C	600°C	1500°C
Final Temperature	320°C	600°C	1500°C	RT
Heating Rate	10°C/min	5°C/min	10°C/min	25°C/min
Hold Time	1 hour	1 hour	3 hours	None

Table 9: The additional pyrolysis processing parameters for the 1300°C 500 micron “mock” CMCs.

Additional 1700°C Graphite Furnace Processing Parameters				
1300°C 500 micron "mock" CMC				
Initial Temperature	RT	320°C	600°C	1700°C
Final Temperature	320°C	600°C	1700°C	RT
Heating Rate	10°C/min	5°C/min	10°C/min	25°C/min
Hold Time	1 hour	1 hour	3 hour	None

These temperature ranges were selected as they are all accepted CMC processing temperatures. This allows for the diffusion of the carbon and silicon into the metal wires to be seen at all different processing temperatures. Figure 25 shows all of the “mock”

CMC samples that were made, the 900°C processed wires without a matrix, the final processing temperature, and the number of iterative PIP cycles they went through.

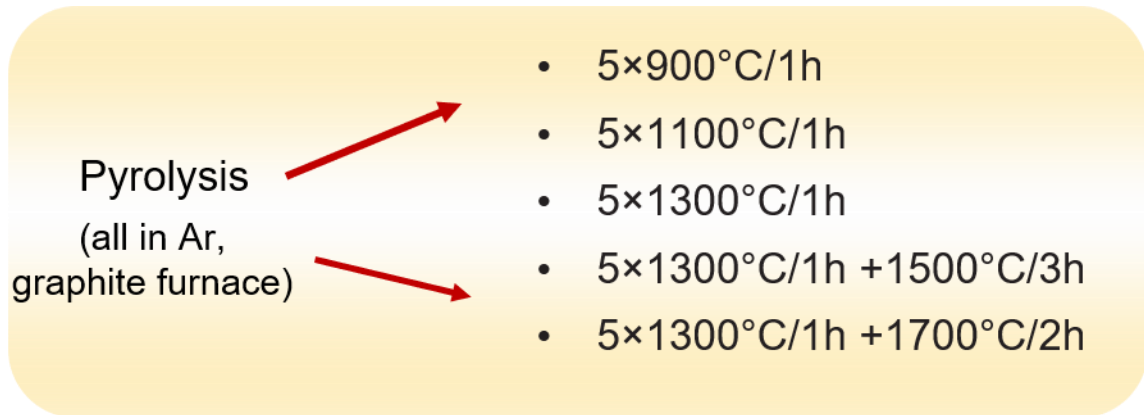


Figure 25: All of the “mock” CMC samples with the iterative PIP processing cycles associated with each sample.

4.1.3 Sectioning and Metallography Preparation

Once the “mock” CMCs were fully processed, they were sectioned in the middle of the sample so the cross section of the wires and the matrix. The sectioned pieces were then placed in a plastic mold and then covered in epoxy (EpoThin™ 2 Epoxy Resin/Hardener; Buehler, Lake Bluff, IL). The 900°C wires were sectioned in half and then mounted in epoxy. Figure 26 shows the sectioned portion of the “mock” CMC that was analyzed. A release agent was used to ensure easy removal. Once the epoxy was cured, each sample went through a grinding and polishing process. An autopolisher (EcoMet 300 Grinder and Polisher; Buehler; Lake Bluff, IL) was used along with various grinding pads (MD Piano; Struers Inc., Cleveland, OH) to grind the sample and prepare it for SEM analysis. The Piano pads that were used were 220 grit to grind away the extra epoxy covering the “mock” CMC sections. Then the 500 grit, 1200 grit, 2000 grit, and 4000 grit Piano pads were used to make the sample clear and ready for analysis. After the progression of Piano pads, a polishing cloth (VerduTex; Buehler, Lake Bluff, IL) and 1

micron diamond slurry (1 μm , Diamond Suspensions – Polycrystalline – Water Based; Allied High Tech Products Inc., Compton, CA) was used to get a final polish on the samples.

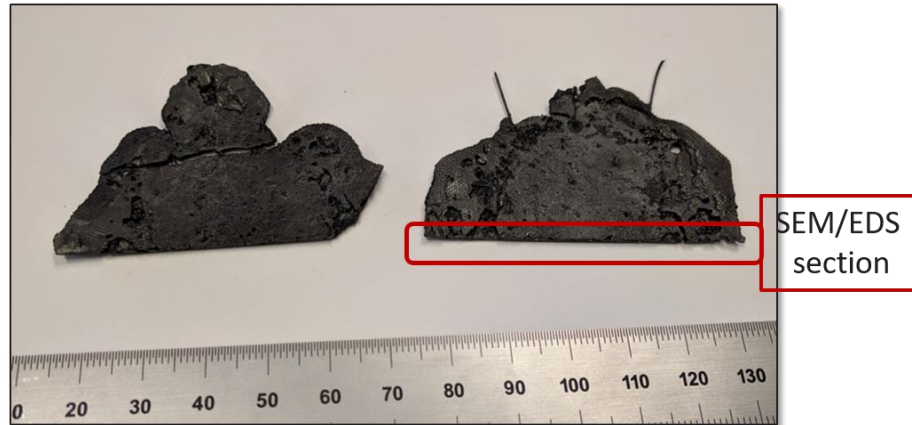


Figure 26: The section portion of the “mock” CMC before being placed in epoxy.

4.1.4 SEM and EDS Characterizations

Once the samples were fully processed, they needed to be coated with a conducting material, so the electrons have a surface to interact with for an image to be generated. Copper tape (3M™ Copper Conductive Tape; Ted Pella, Inc., Altadena, CA) was placed running along the side of the sample to give a connecting point for the electrons to conduct along the sample. The coater (EMS 150T ES; EMS Quorum, Hatfield, PA) sputtered the conducting material, gold platinum, on to the samples. The sectioned samples were then ready for the SEM and EDS analysis.

The samples were analyzed using a Zeiss Gemini SEM and AZtec EDS software. The overall goal of the analysis was to determine if the wires had survived the processing and to see if there was any degradation present.

4.2 Results and Discussion

The 900°C processed wires were analyzed first to ensure that they did survive at the processing temperature. After analyzing all SEM images of the wires, it was determined that the three wires survived the processing. There were no signs of degradation or cracks within the wire. Figure 27 shows SEM images of the three different wires after five cycles of heating in the graphite furnace at 900°C.

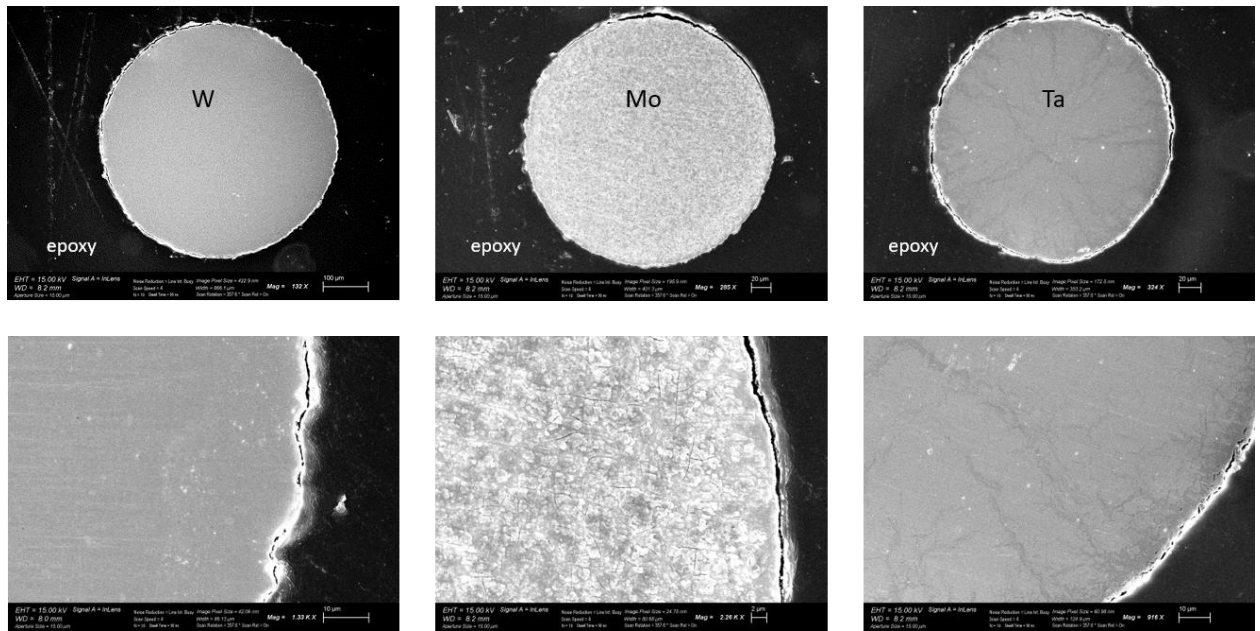


Figure 27: SEM images of the three metal wires after five cycles of heating at 900°C.

After the 900°C wires were analyzed and it was determined that they survived the processing, the four “mock” CMCs were made and processed at 1100°C and 1300°C, then the 1300°C 250 micron and 500 micron composites were processed to an additional higher temperature.

Upon EDS and SEM analysis of the 1100°C, it was determined that all three wires survived the processing. There was no evidence of degradation or diffusion of carbon or silicon into the wires. However, there was evidence of lack of metal to matrix fusion,

resulting in major pores and gaps around the metal wires. Figure 28 shows the three wires after processing for five cycles at 1100°C.

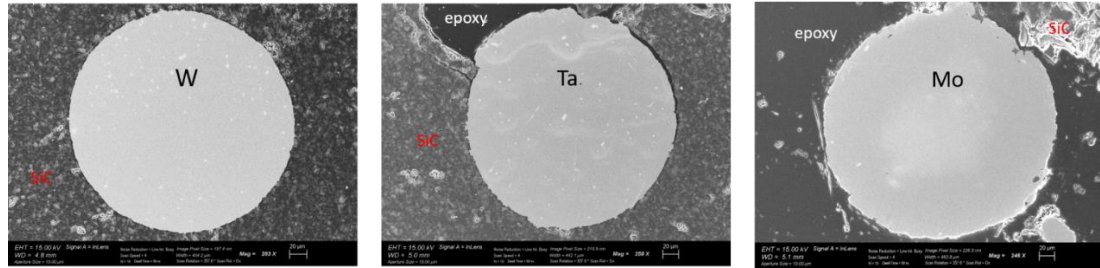


Figure 28: SEM images of the 1100°C “mock” CMC wires after processing.

For the 1300°C “mock” CMC, it was determined that there were signs of degradation in some of the wires. . The edge of the tungsten wire began to show signs of forming a reaction layer. It was very small, but still present. In the SEM image, slight metal to matrix separation can be seen. After EDS analysis, carbon diffusion was present within the tungsten wire. Figure 29 shows the tungsten wire SEM image, carbon EDS map, and silicon EDS map after five cycles at 1300°C.

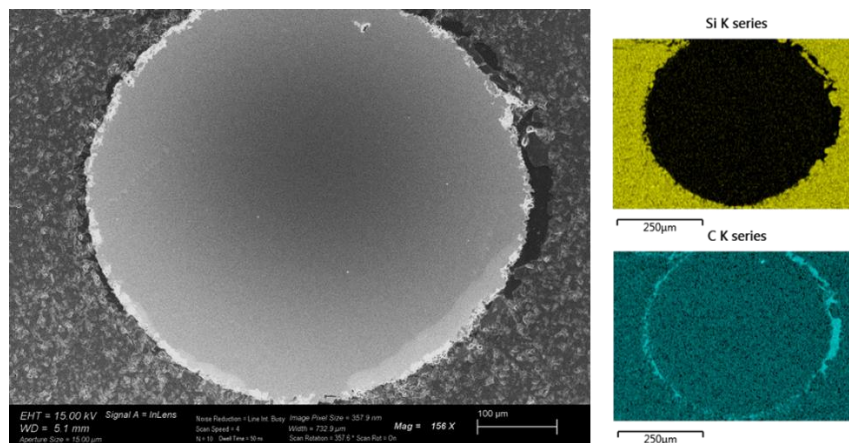


Figure 29: The tungsten wire SEM image, carbon EDS map, and silicon EDS map from the mock CMC after processing at 1300°C.

The molybdenum wire showed signs of aggressive degradation. There was a very evident reaction or diffusion region within the wire. The silicon atoms migrated into the

molybdenum wire. There was also major metal to matrix fusion issues. The entire right side of the wire is not in contact with the matrix. Figure 30 shows the molybdenum wire and the silicon EDS map after five cycles of pyrolysis at 1300°C.

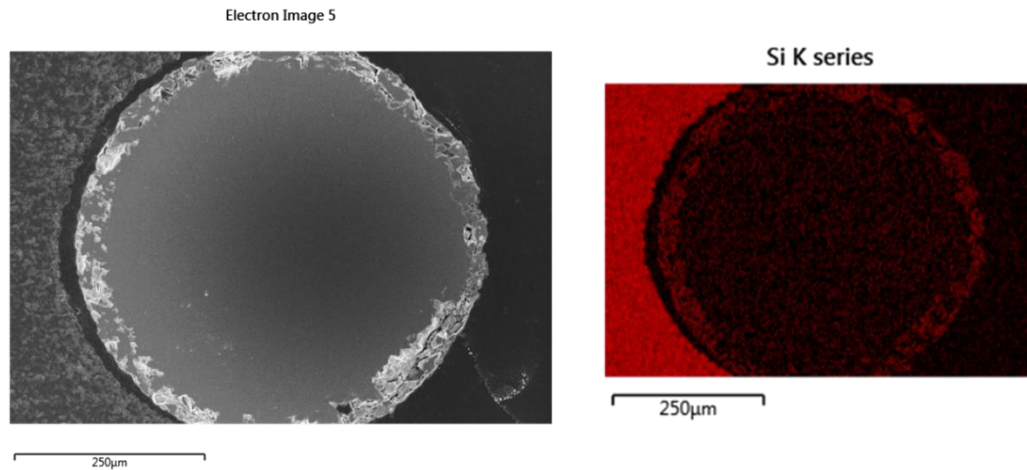


Figure 30: The molybdenum wire SEM image and the silicon EDS map from the mock CMC after five cycles at 1300°C, showing the reaction region within the wire.

The tantalum wire did not show any signs of degradation. Figure 31 shows the tantalum wire SEM image from the mock CMC after five iterative cycle at 1300°C.

After analyzing the 1300°C “mock” CMC, it was decided that the “mock” CMCs needed to be analyzed at higher temperatures to see if there is any progressive reaction layer growth in the molybdenum and tungsten wires and to see if the tantalum wire would start to show signs of degradation. This is when it decided to take the other halves of the 1300°C 250 micron and 500 micron wires to 1500°C and 1700°C to see what happens to the wires.

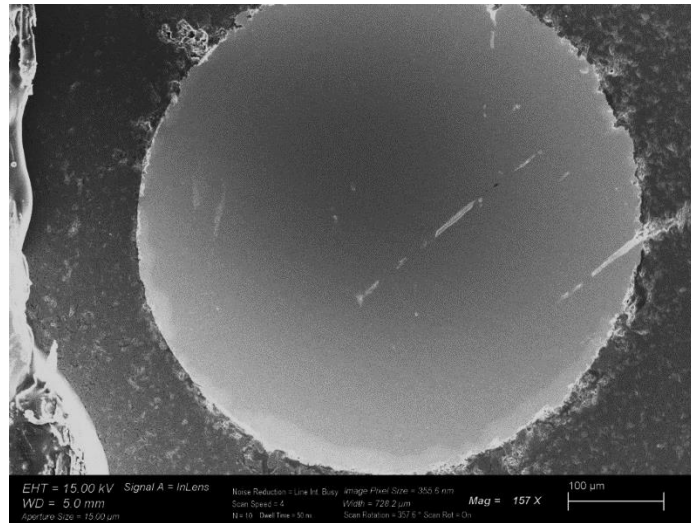


Figure 31: The tantalum wire SEM image from the mock CMC after five iterative cycles at 1300°C, showing no signs of degradation.

Once the additional pyrolysis to 1500°C was done on the 1300°C 250 micron wire composite, it was analyzed by SEM and EDS detector. The tungsten wire showed slightly more of a reaction layer around the surface of the wire. The molybdenum wire showed very similar reaction layer within the wire, but it had grown in size. The tantalum wire still did not show any signs of degradation after processing for the additional temperature and time. Figures 32-34 show SEM images of the tungsten, molybdenum, and tantalum wires in the mock CMCs after the additional 1500°C processing was done to the 1300°C 250 micron composite. There was evidence of metal to matrix adhesion issues in both the tungsten wire and tantalum wire.

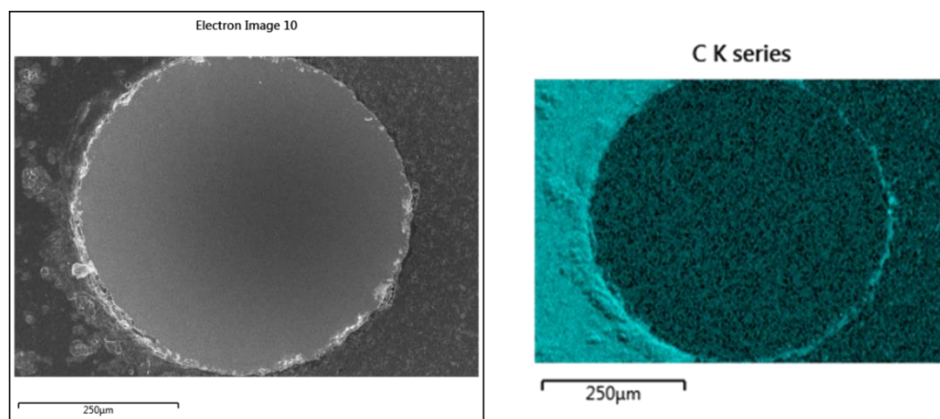


Figure 32: The tungsten wire after the additional 1500°C pyrolysis. The left side of the carbon EDS map shows the major metal to matrix separation.

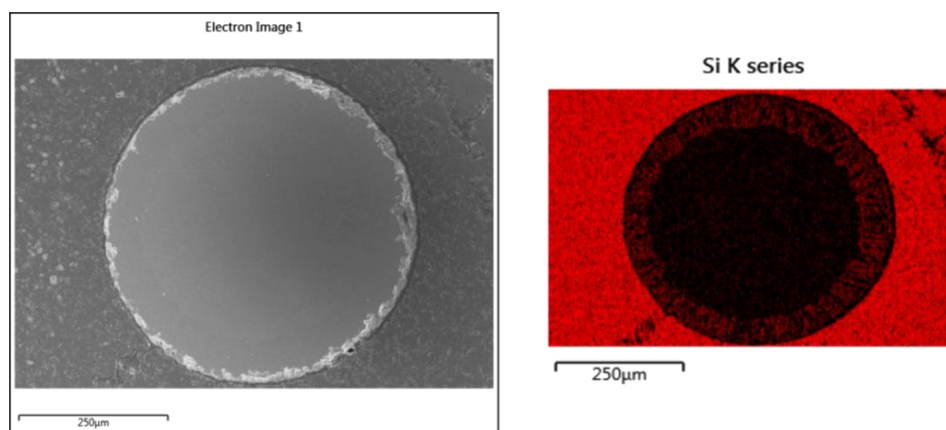


Figure 33: The molybdenum wire after the additional 1500°C pyrolysis. There is a non-uniform reaction zone.

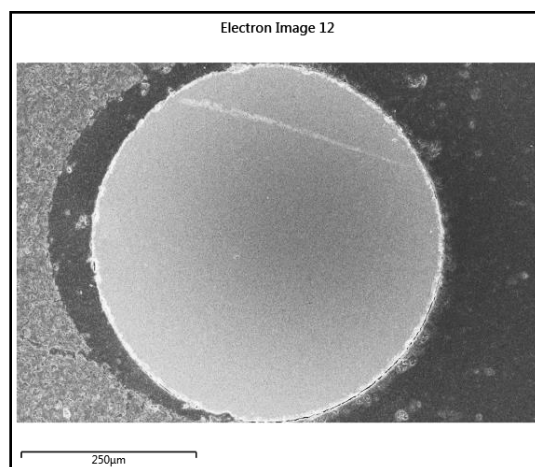


Figure 34: The tantalum wire after the additional 1500°C pyrolysis. There is not any metal to matrix fusion present around the wire.

Additional pyrolysis to 1700°C was done to the 1300°C 500 micron wire composites.

The tungsten wire, in addition to the already seen reaction layer around the surface of the wire, showed clear diffusion zone inside the wire. The diffusion zone cannot be seen when only analyzing the SEM image but it can be seen through the EDS detector. Figure 35 shows the diffusion zone in the tungsten wire.

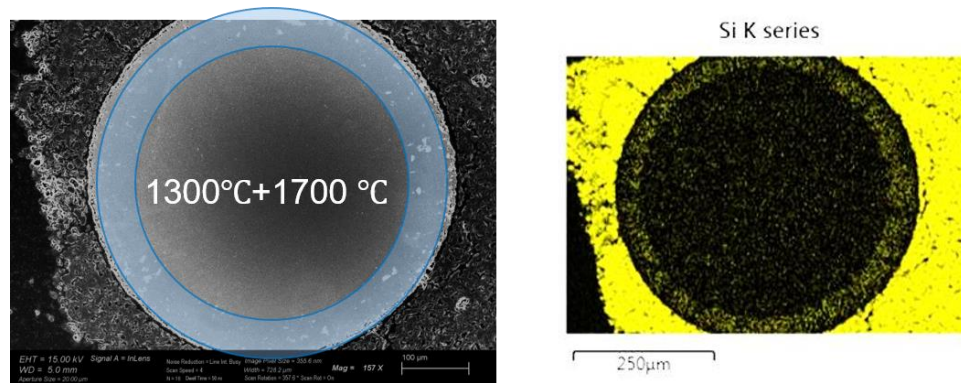


Figure 35: The tungsten wire after the additional 1700°C pyrolysis.

The molybdenum wire showed complete degradation after the additional 1700°C pyrolysis. There was still no physical contact between the metal and the matrix. The diffusion zone within the wire was still non-uniform. Figure 36 shows the diffusion zone within the molybdenum wire after the 1700°C pyrolysis.

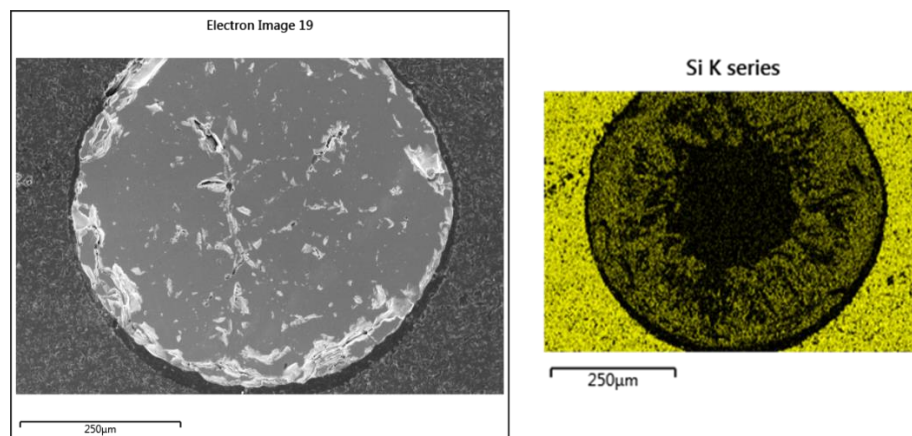


Figure 36: The molybdenum wire after the additional 1700°C pyrolysis.

The tantalum wire began to show some initial signs of degrading after the 1700°C pyrolysis. It was only on the outer surface of the wire and nothing was present within the wire. There was still very little metal to matrix fusion. Figure 37 shows the tantalum wire after the 1700°C pyrolysis.

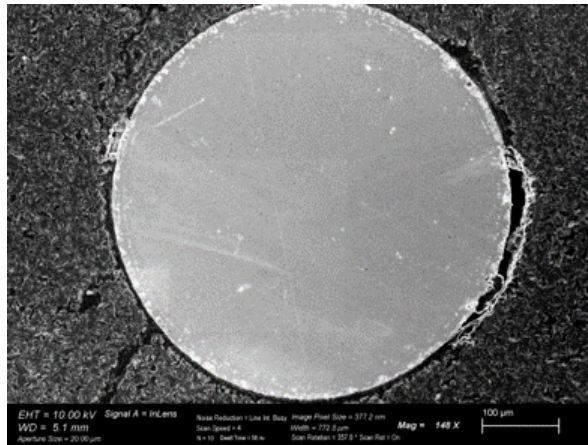


Figure 37: The tantalum wire after the additional 1700°C pyrolysis.

4.3 Conclusions

After analyzing the series of the “mock” CMCs, it was determined that all of the wires survived when processed to 1100°C. Past 1100°C, the molybdenum and tungsten wires showed signs of degradation and diffusion zones. The tantalum wire did not show any degradation until the additional processing at 1700°C. Figure 38 shows which wires survived at each processing temperature. If the metal is green, it completely survived. If it is yellow, it began to show signs of degradation but did not have any major diffusion zones present. Finally, if the metal is red, it showed full degradation and signs of diffusion.

Overall Stability			
Temp. (°C)	Metal		
1100	W	Mo	Ta
1300	W	Mo	Ta
1500	W	Mo	Ta
1700	W	Mo	Ta

Figure 38: The overall stability of the wires at the different processing temperatures.

This study was very informative about how the different common CMC processing temperatures affect the refractory wires when they are in contact with silicon carbide slurry. This study provided information about when each metal began to show signs of degradation and diffusion of silicon and carbon into the different metals. This is important for the final experimental study where the diffusion zones were measured over time at one temperature to see how the diffusion zones changed with time.

However, it does not fully apply to typical CMC processing since it did not include any fiber weaves. The next step was to determine if the fiber weaves being included in the CMC had any effect on the wires.

5. Processing and Characterization of the 1100°C CMC

The ultimate goal of this research is to have metals integrated into the composite without any evidence of degradation or diffusion so the properties of the metals can be utilized.

The next step in determining if a metal can be processed in the CMC to make it functional is adding in the fiber weaves to make it a full matrix. This portion of the research was done to determine if adding in the fiber weaves causes any effect on the survivability of the wires.

The results from the “mock” CMCs showed which processing temperature did not result in diffusion of silicon or carbon into the three different refractory metals and which temperature did result in diffusion from the matrix into the metals. The 900°C and 1100°C “mock” CMCs showed no evidence of migration of carbon or silicon atoms into the refractory metals. The 1300°C “mock” CMC began to show evidence of diffusion into the metals like Mo and W. The 1500°C showed distinct diffusion regions in the Mo and W and the 1700°C showed growth of the distinct diffusion regions in Mo and W as well as evidence of diffusion in Ta. Since the 1100°C “mock” CMC was the only CMC that had all three refractory wires survive the processing parameters, it was chosen as the processing temperature for the new CMC that would include silicon carbide fiber weaves.

5.1 Experimental Aspects

A new CMC would be fabricated, including the silicon carbide slurry, silicon carbide fiber weaves, and the refractory wires. This new CMC would go through iterative PIP cycles to a final temperature of 1100°C.

5.1.1 Layup

The same procedure as described previously was followed for the layup of the 1100°C CMC with minor deviations. The main difference is that the fiber weaves were included in the layup of the CMC. The initial steps of preparing the metal plate for the vacuum bagging and autoclave process was kept the exact same. The layup of the CMC varied from the one described previously.

The same refractory metal wires were used and straightened out by hand. Instead of having two different composites, one with the 250 micron wires and the other with the 500 micron wires, all the wires were placed into one composite together. This composite also included a 460 micron molybdenum wire coated with 2 microns of platinum (Alfa Aesar, Haverhill, MA) and a 250 micron tungsten wire coated with 5 microns of platinum (Alfa Aesar, Haverhill, MA). These wires were initially investigated to see how the platinum effects the diffusion but were quickly disregarded due to the high levels of degradation and diffusion observed.

The fiber weaves were cut from a silicon carbide fiber fabric (Hi-Nicalon™ Type S; COI Ceramics, Inc., San Diego, CA) (8H satin weave, woven by T.E.A.M., Inc., Woonsocket, RI) that were previously coated with boron nitride (BN) and SiC using chemical vapor infiltration (CVI) (Rolls-Royce High Temperature Composites, Inc., Huntington Beach, CA). Four pieces were cut in the warp direction and four pieces were cut in the weft

direction. Figure 39 shows the difference between warp and weft fiber orientation. Each weave was coated in the sample volume percent slurry. A roller (Air Roller 232, Airtech Advanced Materials Group, Huntington Beach, CA) was used to spread the slurry on the weaves and to ensure complete saturation of the slurry into the weave. Once each weave was saturated with the SiC slurry, the layup began.

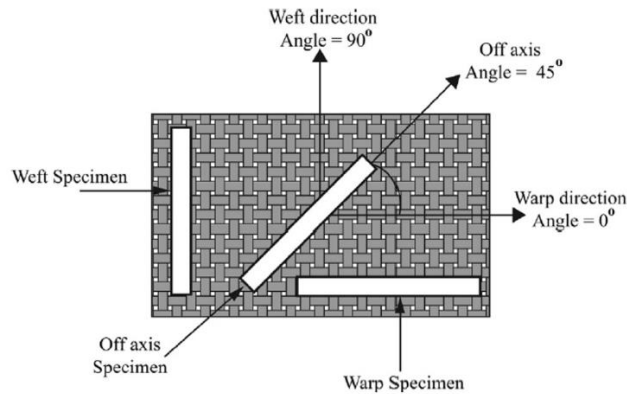


Figure 39: The difference between warp and weft fiber weave orientation; [27].

Two saturated fiber weaves were placed down, warp first and then weft. Then the 250 micron wires were placed onto of the weaves. The wires were spread out to ensure they did not touch, preventing any metal to metal interaction. Extra slurry was poured on top of the wires to ensure they would adhere to the fiber weaves and make a cohesive matrix. Two more fiber weaves were placed on top of the 250 micron wires, following the warp – weft order. The 500 micron wires were placed on top, following the same procedure. After this, the same layup process was repeated with the platinum coated wires. Once all of the metal wires were placed and spaced away from other wires, the final two saturated fiber weaves were placed on top of the stack. The same process was repeated to set up the metal plates and the vacuum bagging for the autoclave run as previously described in 4.4.1. The same processing parameters were used for the autoclave run. Once the CMC

was finished in the autoclave, it was ready for the first pyrolysis cycle and the iterative reinfiltration cycles.

5.1.2 Processing

The processing of the 1100°C CMC was done similarly as described in section 4.4.2. The autoclave processing parameters to ceramicize the silicon carbide slurry, silicon carbide fibers, and metal wires into a CMC is shown in Table 1. The CMC went through the same initial pyrolysis processing, which can be seen in Table 3.

The reinfiltration process varied from what was done for the “mock” CMCs for the 1100°C CMC. The reinfiltration was done in a vacuum oven that was heated to 55°C. The SMP-10 was allowed to warm up to room temperature. The CMC was propped up with wooden sticks, so it did not sit directly on the bottom of the petri dish. Once the CMC was placed on the wooden sticks in the petri dish, the SMP-10 was poured over it, ensuring it was completely covered. The petri dish was placed in the vacuum oven and left to reinfiltrate for about one to two hours. The reinfiltration vacuum oven cure cycle processing parameters are shown in Table 5.

After each reinfiltration cycle, the CMC was pyrolyzed following the processing parameters we the same as the “Mock” CMC shown in Table 6.

After each pyrolysis cycle, the CMC was weighed, and a sample was cut from the main piece. A sample was cut from the CMC after each PIP cycle so each metal could be analyzed during each iterative cycle; determining if there were any minute changes that were not noticed during the “mock” CMC analysis. The weight of the CMC was recorded to calculate the weight percent change from cycle to cycle. Once it reached a weight percent change of below 2%, the PIP processing cycles were ended because it would not

densify much more and would ultimately be a waste of time and resources. Equation 11 shows the weight percent calculation. The CMC was processed for eight iterative cycles, resulting in eight different samples from the CMC.

$$\frac{\text{Weight of composite after pyrolysis 5} - \text{weight of composite after pyrolysis 4}}{\text{Weight of composite after pyrolysis 4}} \times 100 \quad (11)$$

5.1.3 Sectioning and Metallography Preparation

The individual samples taken from the CMC after each PIP cycle were prepared in the same manner as described previously. Figure 40 shows the interface that was polished and analyzed for each sample. The blue rectangle represents the CMC. The red line shows where the cut was made. The black arrows point to the interface that was placed down in the puck for mounting in epoxy and the yellow oval represents the interface that was polished and analyzed for each sample. The inside of the cut was chosen to be analyzed to ensure that any edge effects that might be present near the end of the sample could be ignored. This cutting process was repeated after each PIP cycle. The samples were then mounted in epoxy and polished using Piano pads. Afterwards, they were coated with gold palladium. The samples were then ready for the SEM and EDS analysis.



Figure 40: The interface of each sample that was cut and analyzed using SEM and EDS.

5.1.4 SEM and EDS Analyses

The samples that were taken after each round of the PIP processing were polished and then analyzed using a Zeiss Gemini SEM to obtain images of the wires. The samples were also analyzed using the AZtec X-Max detector to determine if any diffusion of carbon or silicon was present in the wires.

5.2 Results and Discussion

Through EDS and SEM analysis it was determined that the three wires did not experience carbon or silicon diffusion during the PIP processing cycle at 1100°C. There were noticeable differences between the 250 micron wires and the 500 micron wires. The 500 micron wires did not show this metal expansion into the matrix or change in shape from the original circular shape of the as received wires. However, some of the 250 micron wires became misshapen at some point during the process. The circular shape of the wires before processing was no longer seen. Figure 41 shows two different 250 micron wires that were misshapen after processing. The cause for the wires expanding in different regions and in different shapes is difficult to determine with complete certainty with the level of research that was conducted at this point.

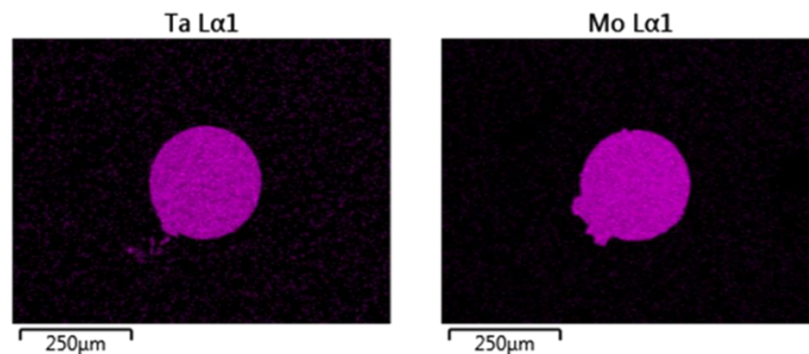


Figure 41: EDS maps of Tantalum and molybdenum 250 micron wires after the 7th PIP cycle showing metal expansion and change from the original circular shape of the wires.

Further studies are needed to determine why the 250 micron wires and the 500 micron wires reacted differently and had different shapes after processing. Assuming the expansion of 250 micron wires is due to the cool down rate of the wires after heating and the differences in the thermal expansion coefficients between the wires and the silicon carbide matrix, it would have also been seen in the 500 micron wires since they went through the same processing parameters. It is now theorized that the greater surface area of the 500 micron wires allowed for better matrix to metal fusion, thus preventing the metal wires from expanding and changing from the original circular shape. Further investigations are needed to fully determine the reason for the difference in the shape of the 250 micron wires after processing.

Regardless of the change in shape after processing for some of the wires, none of the wires, 250 micron or 500 micron, showed any signs of degradation or diffusion of silicon or carbon from the matrix into the wires. Since there was no evidence after any PIP cycle that there was carbon or silicon atoms migrating into the wires, it was concluded that the addition of the silicon carbide fibers did not cause any diffusion of silicon or carbon into the metal wires.

The addition of the fiber weave did improve the overall metal to matrix fusion. The level of separation between the metal wires and the silicon carbide matrix in the “mock” CMCs was not seen in the fully processed 1100°C CMC. There are still pores and cracks within the CMC that can be seen near some of the wires, but this is common for PIP processed CMCs.

Figure 42 shows the final EDS maps taken for the 500 micron wires for the carbon, silicon, and metal wire content. Some of the pores can be seen in the EDS maps. The

pores filled with epoxy during the sample preparation cycle, so the pores appear red in the carbon EDS maps for each wire. The silicon EDS maps are shown in a light blue color. The carbon EDS maps are shown in red. The molybdenum EDS map is shown in green. The tantalum map is shown in yellow and finally, the tungsten EDS map is shown in orange. The top row of images in Figure 42 corresponds to the 8th cycle 500 micron molybdenum wire. The middle row of images corresponds to the 8th cycle 500 micron tantalum wire and the last row of images corresponds to the 8th cycle 500 micron tungsten wire.

The EDS maps for the tantalum and molybdenum wires shows some silicon and tantalum/molybdenum overlap when looking at the silicon map. This is not representative of silicon migrating into the metal wires or of a new silicide phase forming with the metal wires. This overlap is present in the silicon EDS maps because the tantalum and tungsten $M\alpha$ signals overlap with the $K\alpha$ signal from silicon. The $M\alpha$ signal for tantalum is 1.7096. The $M\alpha$ signal for tungsten is 1.7744. The $K\alpha$ signal for silicon is 1.7398 [28]. These signals are too similar to be accurately separated. This is why there are signs of silicon in the tungsten and tantalum wires without there being any silicon diffusion or silicide phase formed.

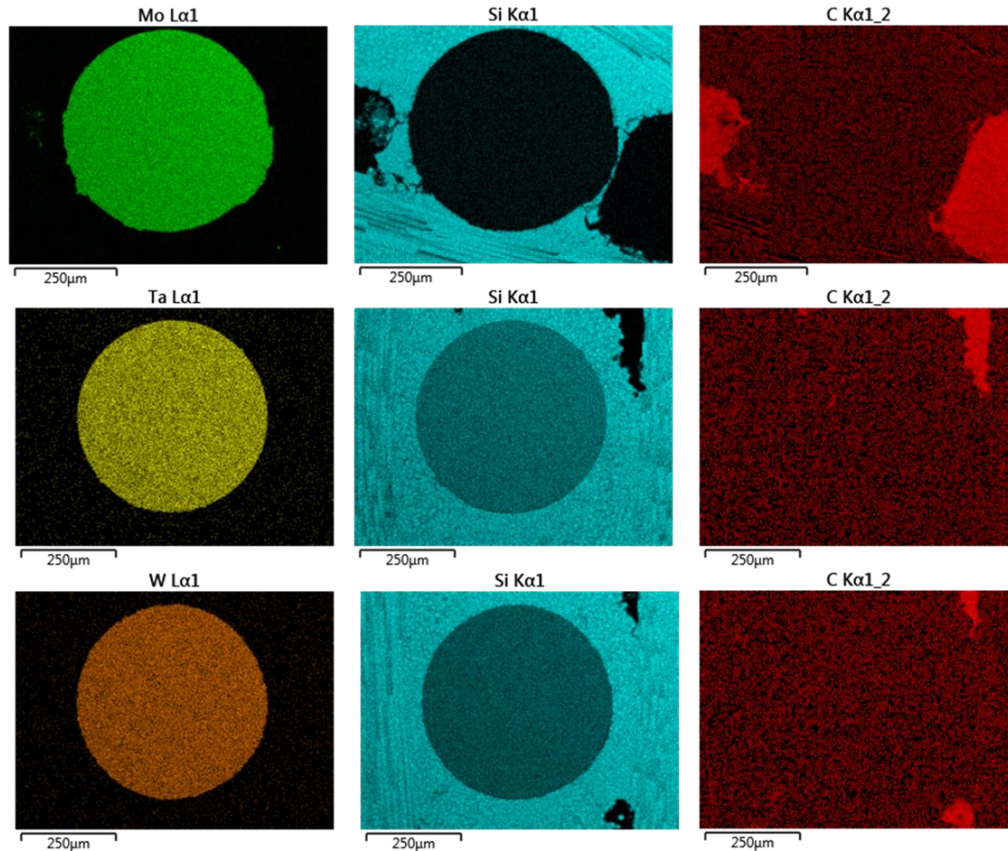


Figure 42: The final EDS maps taken for each wire after eight cycles of PIP processing.

5.3 Conclusion

The 1100°C CMC with the addition of the silicon carbide fiber weave completely survived the eight cycles of PIP processing. Some of the 250 micron wires showed expansion into the matrix and an overall change in shape during different processing cycles. This was not seen in the 500 micron wires. Further investigated is needed to determine the cause for this, but it is theorized that the greater surface area allowed for better metal to matrix fusion, thus preventing the 500 micron wires from expanding and changing from the original circular shape. The addition of the fiber weaves improved the overall metal to matrix fusion. There were still pores present in the CMC, but that is common and expected with PIP processing. There was no evidence of carbon or silicon

diffusion into the three metal wires. All three wires survived the processing and showed no signs of degradation.

Due to the lack of silicon or carbon diffusion into the metal wires, it was concluded that tungsten, tantalum, and molybdenum could be added to a SiC/SiC CMC without effecting the overall cost or processing time. Since the processed 1100°C CMC survived, showing no signs of degradation or diffusion, and did not add cost or time to the processing, it was determined that 1100°C would be the temperature at which a new CMC would be processed.

6. Si and C Diffusion Study in a CMC at High Temperatures

After determining that the addition of silicon fiber weaves did not result in diffusion or degradation within any of the refractory wires during the 1100°C PIP processing CMC, the next step was to force diffusion of silicon and carbon into the metal wires. The goal of this tertiary experiment was to determine the diffusion coefficient and activation energy of the diffusion that was occurring within the metals. As previously mentioned, the diffusion zone was too small in size to be analyzed using XRD analysis, so the phase that was forming was not able to be determined. However, by heating the non-degraded CMC to elevated temperatures and measuring the growth of the diffusion zone in each wire, the activation energy and diffusion coefficient for the phase could be determined through manipulation of the Arrhenius equation.

The newly processed CMC would then be exposed to additional cycles at higher temperatures to attempt to map out the diffusion of carbon or silicon into the metal wires. The additional higher temperature cycles would be done in hour long increments so the diffusion zone into the metal wire could be seen as a step-wise and time dependent function. The Arrhenius function equation would then be applied to determine the activation energy and diffusion constant for each of the metals.

The Arrhenius equation, as shown previously in Equation 9, involves the diffusion rate coefficient, K , the activation energy, Q , the gas constant, R , and the final processing temperature, T . The growth rate of the newly formed phase within the metals is a diffusion controlled process. Due to this growth rate being a diffusion controlled process, the diffusion rate coefficient can be determined by measuring the thickness of the formed diffusion zone and applying it to the diffusion rate equation, shown previously in Equation 10.

A new CMC was created, and PIP processed to 1100°C. After the CMC went through eight PIP processing cycles, it was sectioned in half. One half was saved for future testing, potentially altering the time spent at certain temperatures, and the other half went through additional iterative graphite furnace cycles. The portion of the CMC that was additional heated was heated to 1500°C. The CMC was not reinfiltrated between each heating cycle in the graphite furnace. The purpose of this was to see what happens within each wire at elevated temperatures of the fully processed CMC. This replicates a CMC in use, thus demonstrating what would happen to the wires actually embedded in an applied CMC. Each time the CMC was placed in the graphite furnace, it was held at 1500°C for 1 hour. The slowest heating rates and cool down rates were used to prevent separation of the matrix from the metal caused by the differences in the coefficients of thermal expansion. A portion of the CMC was then sectioned off, polished, and analyzed using SEM, EDS detectors, and Raman spectroscopy. The SEM and EDS analysis were used to determine the level of degradation of each wire and the silicon diffusion thickness present. The Raman spectroscopy analysis was used to determine the carbon migration, if any, towards the wire since the EDS detectors have limitations in carbon detection. After

a section was cut from the CMC, it was processed again at 1500°C for 1 hour, then the process was repeated. This created samples that had different exposure time at the same temperature, thus allowing for the diffusion rate equation to be applied to determine the diffusion rate coefficient. The diffusion rate coefficient was then used in the Arrhenius equation to determine the diffusion constant and the activation energy for the diffusion zone present within each metal.

6.1 Experimental Methodology

6.1.1 Layup

The layup process for the new 1100°C CMC was very similar to the layup for the previously described and tested 1100°C CMC. The only difference between the two CMCs was the preparation of the fiber weaves. In the newly processed 1100°C CMC, the fiber weaves were B-staged. This was done to help with the overall struggles of trying to place the fiber weaves over the metal wires without everything shifting. When laying up the previous 1100°C CMC, the fiber weaves and the metal wires would shift continuously, requiring multiple people to help hold everything in place. By B-staging the fiber weaves, it helped to prevent the fiber weaves stay in place and not result in areas with major fiber loss. This allowed for the layup to be done by one person.

After the fiber weaves were B-staged, they were placed between two sheets of Teflon paper. Extra SMP-10 and silicon carbide slurry was placed on each side of the fiber weave in the Teflon paper to ensure that it remained wet overnight. The weaves were then placed in the freezer overnight and taken out the next morning to warm to room temperature before the layup began. Figure 43 shows the preparation of the fiber weaves in the Teflon paper before they were placed in the freezer.

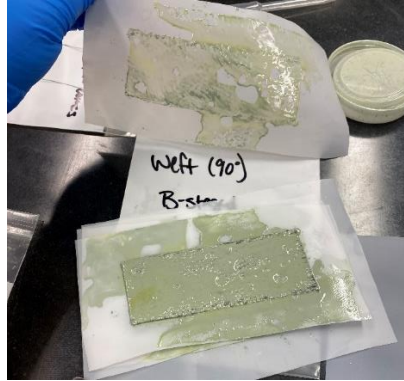


Figure 43: The fiber weaves after B-staging and being prepared for freezer storage.

Once the fiber weaves were warmed up to room temperature, the layup of the CMC began. Everything was kept the same as previously mentioned. The only difference was the wires' position in between the weaves. After two layers of the weave were placed, two 500 micron molybdenum wires were placed down. Then two more weaves were placed, two 500 micron tantalum wires were placed in between the weaves. Another two layers of weaves were laid on top of the tantalum wires, and then two 500 micron tungsten wires were placed on top of the stack. Finally, the last two fiber weaves were placed on top of the stack. Figure 44 shows the final CMC layup and Figure 45 shows the layup schematic.



Figure 44: The final CMC layup of the 1100°C CMC.

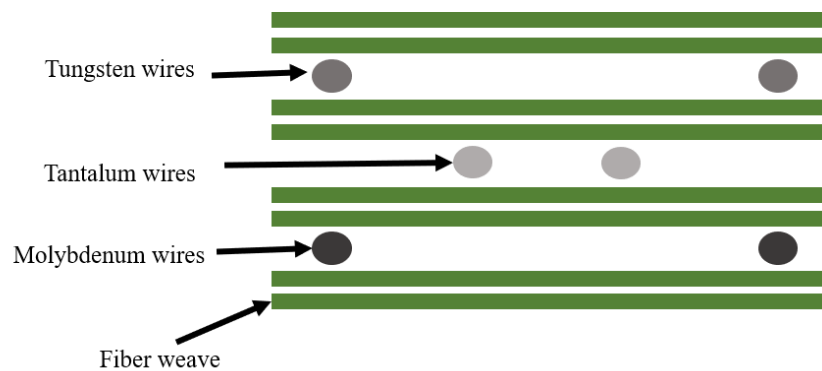


Figure 45: The final CMC layup schematic.

The fiber weaves and wires were then placed on the previously described plate for the autoclave process. The same materials and placement were used as previously described. The sample was prepped and ready for the autoclave to cure the composite together.

6.1.2 Processing

The layup was then placed in the autoclave. The processing parameters were the same as used for the “mock” CMCs and the 1100°C CMC. The autoclave was done to ceramicize the pre-ceramic polymer slurry and form it into one piece. The autoclave processing parameters are shown in Table 1.

After the CMC was removed from the autoclave, it went through the first graphite furnace pyrolysis cycle. The first pyrolysis cycle was the same as the one used for the “mock” 1100°C CMC and the previously processed 1100°C CMC. The first pyrolysis cycle can be seen in Table 10.

Table 10: The 1st cycle graphite furnace processing parameters.

1st Cycle 1100°C CMC Graphite Furnace Processing Parameters					
Initial Temperature	RT	250°C	320°C	600°C	1100°C
Final Temperature	250°C	320°C	600°C	1100°C	RT
Heating Rate	10°C/min	10°C/min	5°C/min	10°C/min	25°C/min
Hold Time	None	1 hour	1 hour	1 hour	None

After the first pyrolysis, the CMC went through the reinfiltration process. The CMC was reinfiltrated using a three gallon vacuum oven from SlickVacSeal. The vacuum oven was set to 60°C. This differed from the previous reinfiltration of the other 1100°C CMC because the temperature would vary due to the size of the chamber, so a higher temperature was chosen to ensure that the overall temperature did not drop too low. The SMP-10 was allowed to warm to room temperature and then was added into the vacuum chamber. Once the SMP-10 and the vacuum chamber reached temperature, the CMC was added in and the vacuum was pulled. The CMC was left to infiltrate for three hours. Figure 46 shows the CMC in the vacuum chamber.

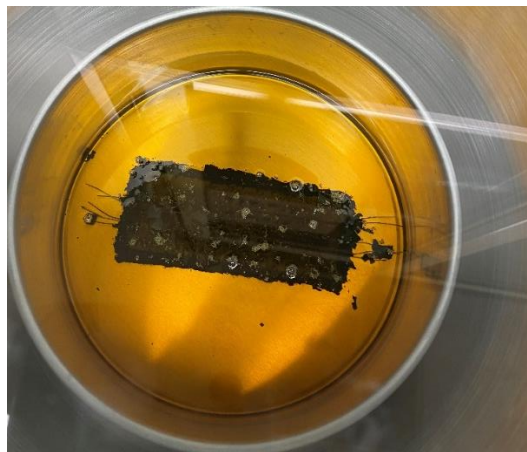


Figure 46: The CMC in the SMP-10 during reinfiltration.

Once the reinfiltration was done, the sample was removed from the vacuum chamber, dried off, and placed in a vacuum oven to cure the SMP-10 in the pores. Figure 47 shows the CMC after reinfiltration ready to be put in the vacuum oven.

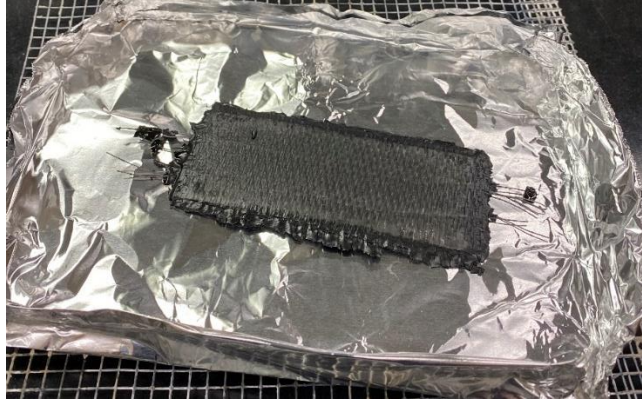


Figure 47: The CMC after the reinfiltration and ready for the vacuum oven to cure the SMP-10 in place in the pores.

The vacuum oven processing parameters can be seen in Table 11. There is a difference in the vacuum oven run from what was done with the previous samples. This was done to save time. The curing of the SMP-10 occurs below 300°C, so this was done to help save time during the lengthy process.

Table 11: The iterative vacuum oven curing run.

Iterative CMC Vacuum Oven Processing Parameters		
Initial Temperature	RT	300°C
Final Temperature	300°C	RT
Heating Rate	2°C/min	2°C/min
Hold Time	1 hour	No hold

Once the vacuum oven run was done, the samples were placed in the graphite furnace and the pyrolysis parameters in Table 6.

This was repeated eight different times until the weight percent change was below two percent. Once this was done, the sample was taken to 1500°C and held for 1 hour. This was done without a reinfiltration process between the graphite furnace runs. Table 12 shows the heating parameter to 1500°C. The additional heating was done to force the diffusion to occur within the metals.

Table 12: The additional 1500°C processing parameters.

Additional 1500°C Pyrolysis CMC Graphite Furnace Processing Parameters				
Initial Temperature	RT	320°C	600°C	1500°C
Final Temperature	320°C	600°C	1500°C	RT
Heating Rate	10°C/min	5°C/min	10°C/min	10°C/min
Hold Time	1 hour	1 hour	1 hour	None

6.1.3 Sectioning and Metallography Preparation

After the 1100°C processing was done the CMC was sectioned in half. One half went through the additional 1500°C heating and the other half was saved for future testing. After each 1500°C heating, a small sample was taken and then mounted and polished as previously described. The sample was then prepared for SEM and EDS analysis by placing copper tape and iridium coating on the surface. The sample was then analyzed. While the sample was getting prepared for SEM and EDS analysis, the rest of the CMC was heated again to 1500°C. The process was repeated four different times so the diffusion zone growth could be measured.

6.2 Results

After each additional heating cycle of the newly processed 1100°C CMC, a small section was cut from the CMC. This was then mounted in epoxy and polished for SEM and

Raman spectroscopy analysis. Figure 48 shows a drawing of the CMC. The blue portion is the part that was sectioned off after each additional 1500°C heating. The red line shows where the cut was made and what face of the sample was mounted down and polished. The black portion of the CMC went through the next round of 1500°C heating. The process of sectioning the CMC was repeated after each additional heating cycle.



Figure 48: A model of how the CMC was sectioned after the additional 1500°C heating cycles.

Once the samples were polished, SEM and EDS analysis were done on the samples. An image was taken of the entire wire to see how the heating had affected the wire. Each wire was broken into four sections; top, bottom, left, and right. Each section was imaged at a higher magnification to see the matrix to wire adhesion and any potential diffusion zones or degradation due to the additional heating. In each small section of the wires, EDS analysis was done to determine the silicon content within the wire, if any was present. EDS maps and linescans were collected. The maps proved were useful in showing any overall diffusion by marking each element present in the image with a different color. The linescans were useful in determining the actual length of the diffusion zone in the wires, if there was any present. As mentioned previously, there is a significant overlap in the signals from tungsten and tantalum with the signal from silicon. To remedy this issue and accurately represent where the silicon content is actually present in each sample, the tru-map and tru-line function was used on the AZtec software. This allowed

for a more distinct differentiation between the silicon signal and the tantalum and tungsten signals.

When analyzing the SEM and EDS data, it was determined that the only wire that showed diffusion due to the additional heating was the molybdenum wire. The tungsten and tantalum wires did not show any diffusion after any cycle of additional heating. The edges of the tantalum and tungsten wires began to show some signs of degradation, but no diffusion was seen in either wire. The matrix to wire adhesion was of poor quality in all three wires, showing signs of separation. Figures 49 and 50 show the tantalum and tungsten wires, respectfully, after the four additional heating cycles to 1500°C. The images are distorted on the edges due to the low magnification needed to image the whole wire. The Zeiss SEM that was used is meant for very high magnification imaging. The edges of the wires show signs of degradation.

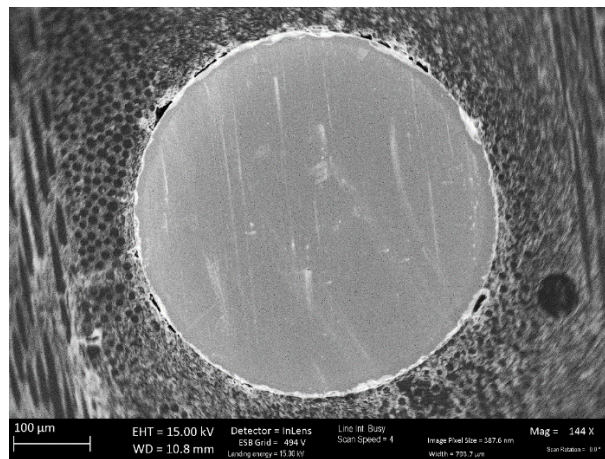


Figure 49: The tantalum wire after four additional heating cycles to 1500°C.

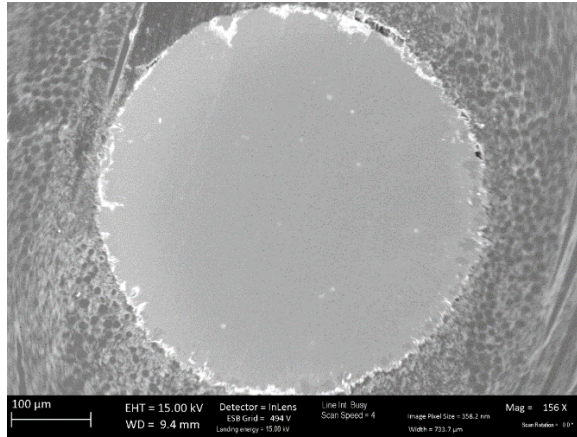


Figure 50: The tungsten wire after four additional heating cycles to 1500°C.

The edge of both wires looks like it may be showing signs of diffusion by just analyzing the SEM images. However, when the EDS linescans were analyzed, it was shown that there was no presence of carbon or silicon in the wire. Figures 51 and 52 show the tantalum and tungsten wires' linescans. There is a specific drop off of the silicon signal when transitioning from the matrix to the metal. Once the scan was in the metal, it was only showing signal from the metal wires.

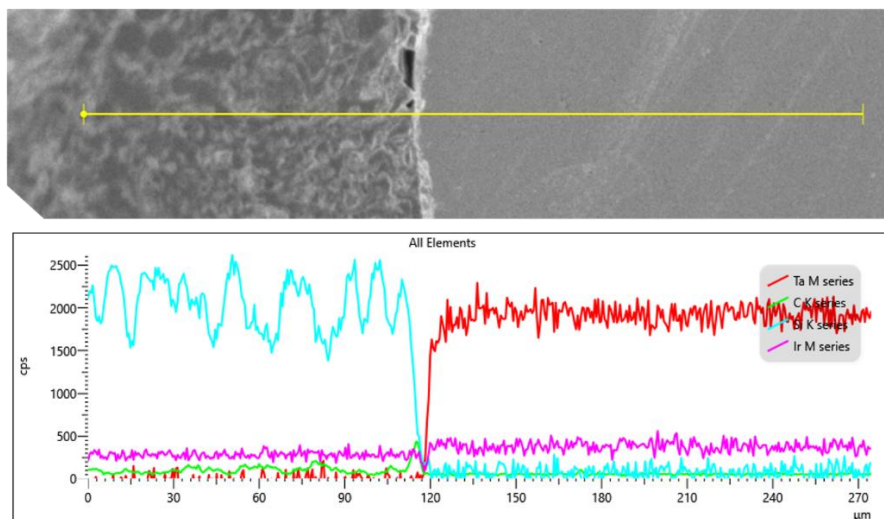


Figure 51: The tantalum wire EDS linescan after four cycles of the additional 1500°C. The red line represents that tantalum signal, and the light blue line represents the silicon signal.

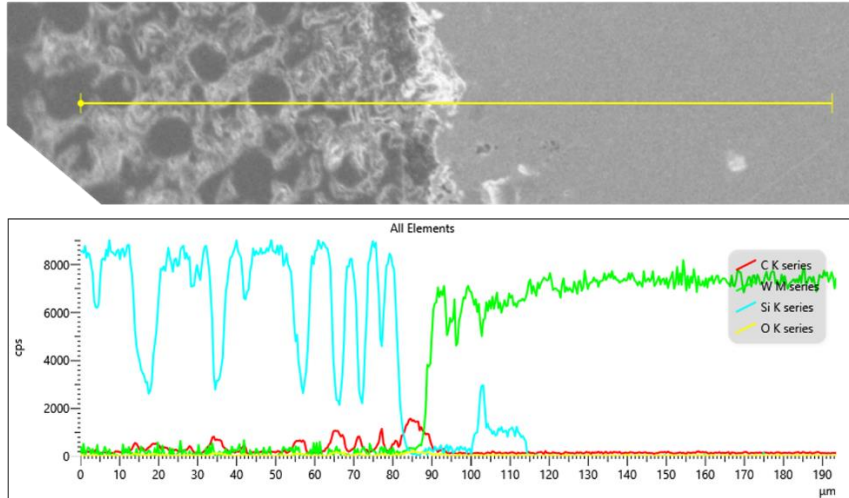


Figure 52: The tungsten wire EDS linescan after four cycles of the additional 1500°C. The green line represents that tungsten signal, and the light blue line represents the silicon signal.

After the first cycle of additional heating, the molybdenum wire began to show signs of silicon diffusion. The silicon could be seen in the wire in EDS maps and EDS linescans. Figure 53 shows the EDS maps for the four different sections of the molybdenum wire after two hours of additional heating. The silicon diffusion zone present in the molybdenum wires is non-uniform in nature, varying in overall length from place to place within the wire. Some places showed much larger diffusion zones while others showed smaller diffusion zones.

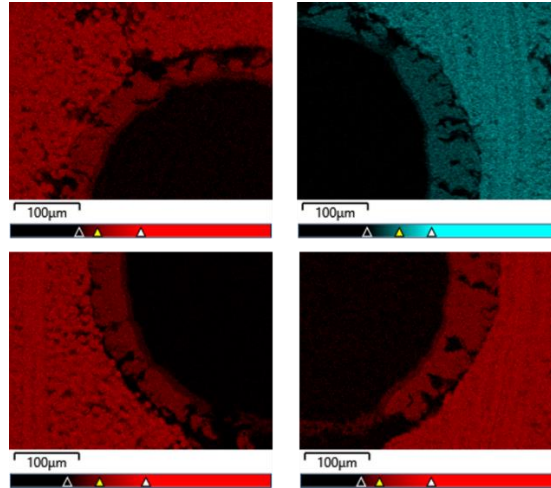


Figure 53: The silicon diffusion into the molybdenum wire after two hours of additional heating.

The length of the silicon diffusion into the wire was calculated by analyzing the linescan data and measuring the signal overlap between the molybdenum wire and the silicon.

Figures 54, 55, 56, and 57 show one section of the molybdenum wire's EDS linescan data after each additional heating cycle. Figure 54 shows the linescan after one heating cycle, Figure 55 shows the linescan after two heating cycles, Figure 56 shows the linescan after three heating cycles, and Figure 57 shows the linescan after four heating cycles.

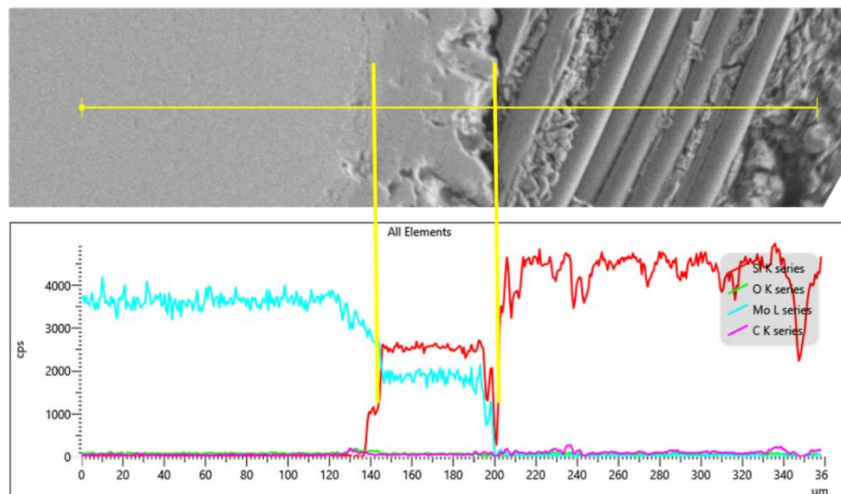


Figure 54: The linescan from the molybdenum wire after one hour of additional heating to 1500°C. The red line represents the silicon signal, and the light blue line represents the molybdenum signal.

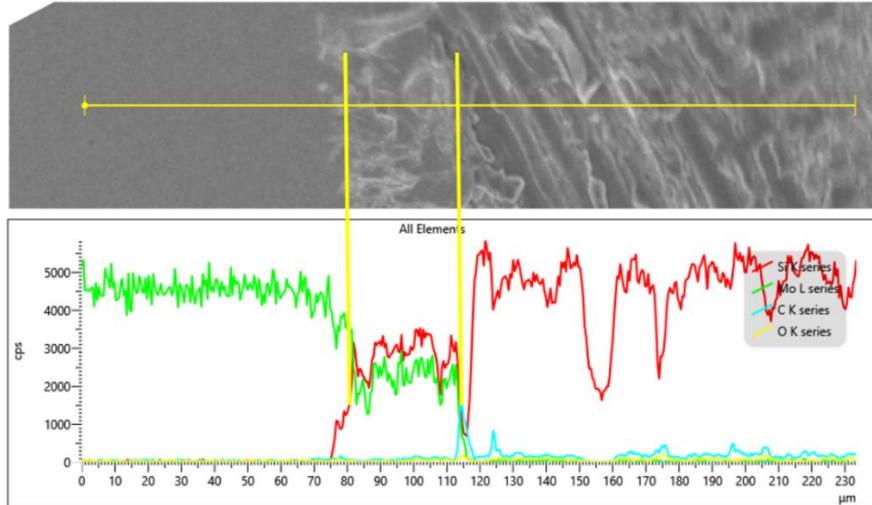


Figure 55: The linescan from the molybdenum wire after two hours of additional heating to 1500°C. The red line represents the silicon signal, and the green line represents the molybdenum signal.

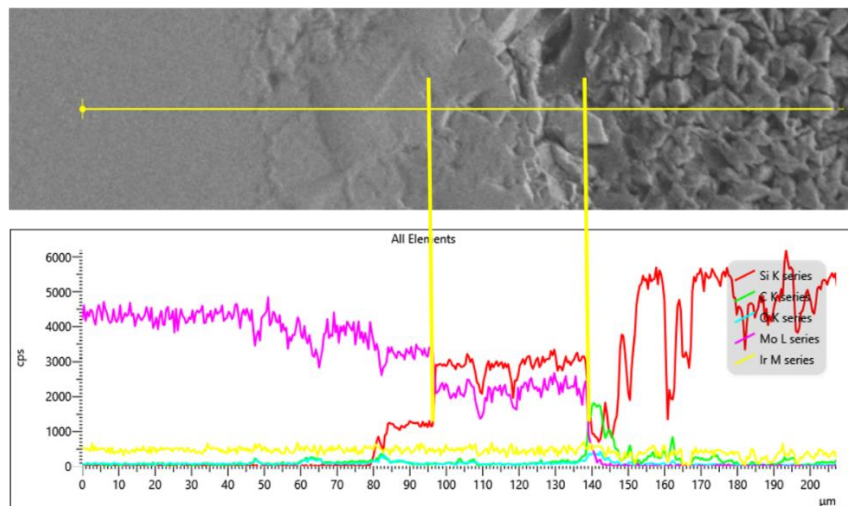


Figure 56: The linescan from the molybdenum wire after three hours of additional heating to 1500°C. The red line represents the silicon signal, and the purple line represents the molybdenum signal.

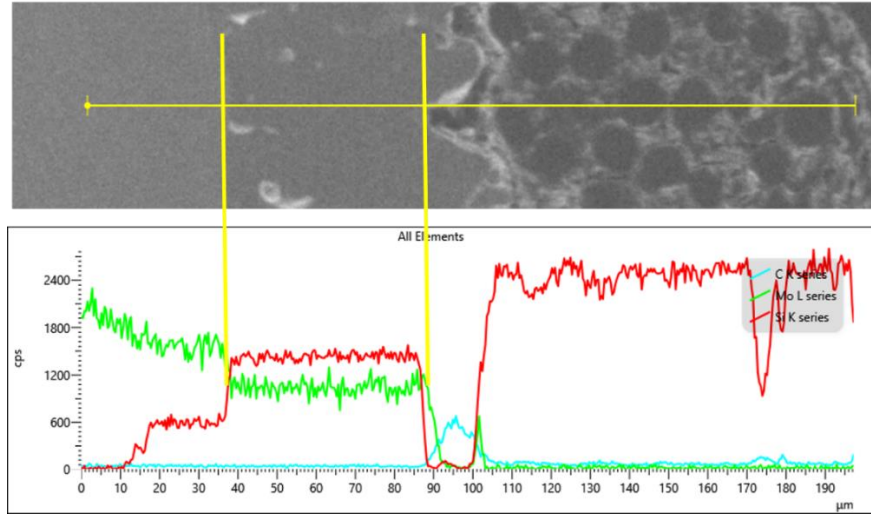


Figure 57: The linescan from the molybdenum wire after four hours of additional heating to 1500°C. The red line represents the silicon signal, and the green line represents the molybdenum signal.

The bolded yellow lines connect the main overlap between the silicon signal and the molybdenum signal to the portion of the metal where it is coming from. However, there is also a smaller region of silicon signal overlapping with the molybdenum signal, this can be seen in Figures 56 and 57. Figure 56 also shows an interested region where the signal for silicon is not present, but the wire still shows signs of degradation. This needs further research to fully determine the impact of this result, but shows that the molybdenum wire also degrades at 1500°C without direct signal of silicon being present in the area of degradation.

The x axis for all of the linescans show the length measured in microns. The overlap region represented the diffusion thickness. For each heating cycle, there were four linescans, one from each section. The diffusion thickness was recorded for each linescan, and then they were averaged together. When the main overlapping signal, as represented by the yellow lines, is averaged for each heating cycle, the results are as follows:

1500°C/1h has an average diffusion zone of 27.75 microns, 1500°C/2h has an average

diffusion zone of 53 microns, 1500°C/3h has an average diffusion zone of 50 microns, and 1500°C/4h has an average diffusion zone of 54.75 microns. After two hours of additional heating, the diffusion zone did not seem to have any further diffusion growth.

However, when all of the silicon signal is included in the averaging for the diffusion length after each heating cycle, the results are as follows: 1500°C/1h has an average diffusion zone of 25.75 microns, 1500°C/2h has an average diffusion zone of 57.75 microns, 1500°C/3h has an average diffusion zone of 61 microns, and 1500°C/4h has an average diffusion zone of 66.25 microns. The average calculated is not necessarily the best representation of the diffusion zone length due to the significant difference in diffusion zone length from one place to another within the same wire. This is due to the non-uniformity of the diffusion zone thickness throughout the wire. An example of the non-uniform diffusion zone thickness in the same sample can be seen in Figure 58. The top linescan shows the 1500°C/4h sample with a diffusion zone of 71 microns and the bottom linescan shows the 1500°C/4h sample with a diffusion zone of 51 microns.

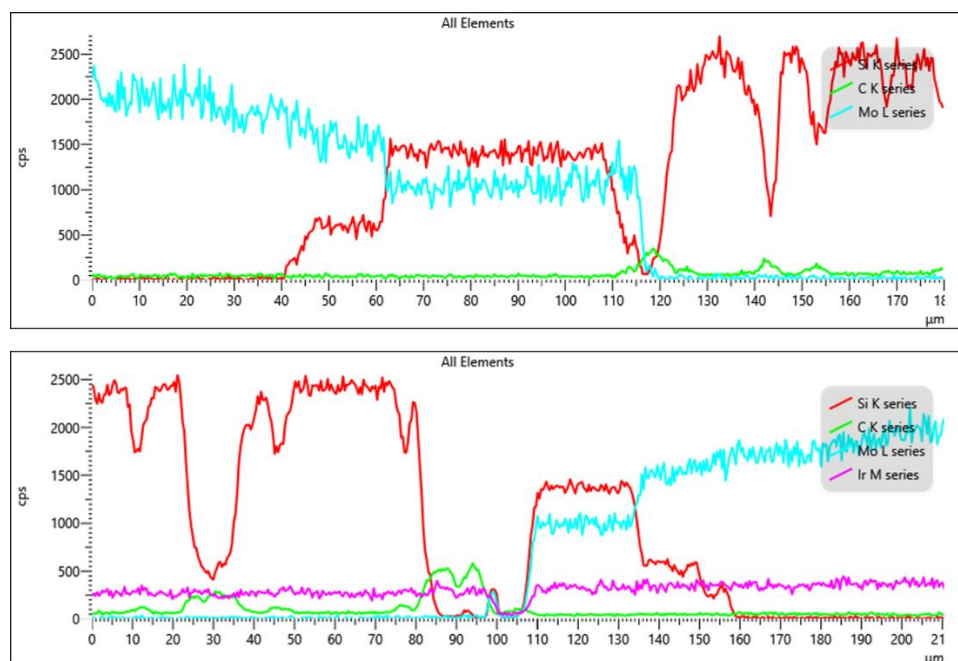


Figure 58: The differences in diffusion zone thickness within one sample (1500°C/4h).

The diffusion thickness average, including all of the silicon and molybdenum overall, for each time was plotted against the time spent at 1500°C in a logarithmic plot. By plotting the log of the thickness of the diffusion zone by the log of the time spent at 1500°C, the time dependence of the diffusion could be analyzed. The slope of the plot determines the time dependence. If the slope is one, then the diffusion growth is reaction rate controlled. If the slope is one half, then the diffusion growth is controlled by diffusion through scale. Figure 59 shows the plot of log of the thickness of the diffusion zone versus the log of the time spent at temperature. The slope is 0.6822, meaning that the time dependence of the diffusion zone forming is not able to be determined with the current amount of data points. When analyzing just the diffusion thickness growth from 1 hour to 2 hours at 1500°C, the slope is 1.1652. This value is much closer to 1, resembling reaction rate time dependency. However, for the whole experiment, no conclusions can be made about the

time dependency. Further analysis and data are needed to determine any diffusion information due to the non-uniformity of the diffusion zone present within the wires.

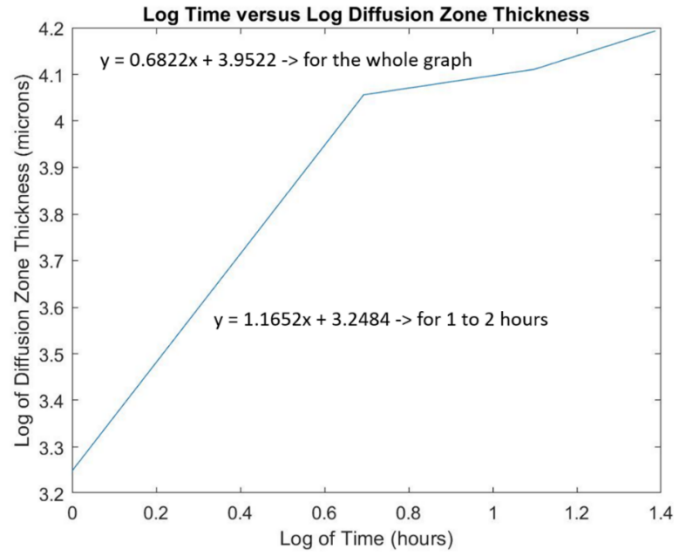
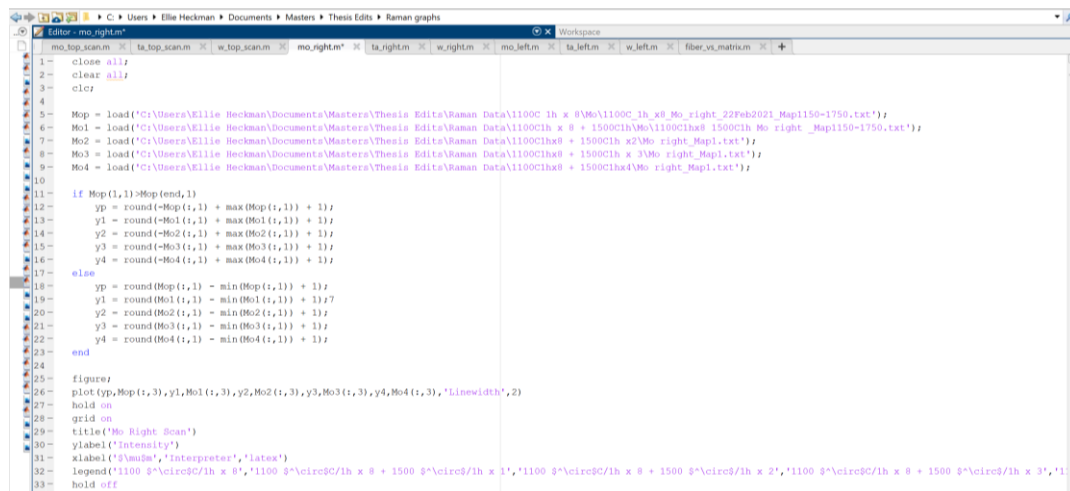


Figure 59: The time dependency plot for the diffusion thickness versus time.

The other system in contact with the molybdenum, tungsten, and tantalum wires was the carbon from the silicon carbide. To measure the carbon content, Raman spectroscopy was used since the EDS has limitations in reading the carbon content present within a sample. The Raman analysis was done on the samples to determine the carbon content and movement during the additional heating cycles. Carbon has two different peaks that appear during Raman spectroscopy, one around 1400 and 1600 cm^{-1} . By measuring the intensity of the carbon peaks throughout the sample, the areas with carbon present can be determined. There were four regions of each wire analyzed; the top, bottom, left, and right. This was done for each sample that was taken after the additional heating cycles and for the sample that was taken after the initial processing to 1100°C. The software had the ability to do a base to signal analysis. This allowed for a specific region, 1150 to 1750 cm^{-1} , to be analyzed and determined the intensity of the carbon over a length of sixty

microns. Sixty microns was chosen to represent a portion outside of the wire and a portion within the wire.

This method of analysis did have its limitations. The software input a line of best fit between the two regions and then the area above the line was measured. The placement of the line of best fit was not controllable, so it resulted in some values being negative in signal due to the data being below the line of best fit. The intensity data and the position in the sample, one micron being outside the wire and sixty microns being within the wire, were exported. A MatLab code was written to analyze each region of data for each wire, resulting in twelve different codes. There was a code for the top region in all molybdenum wires, the right region in all the molybdenum wires; this continued until there was a code for each section of each wire. The code overlaid all of the data collected for one region of each wire. For example, the molybdenum top region code, it included the data from the 1100°C x 8 sample, the 1100°C x 8 + 1500°C x 1 sample, the 1100°C x 8 + 1500°C x 2 sample, the 1100°C x 8 + 1500°C x 3 sample, and the 1100°C x 8 + 1500°C x 4 sample. Figure 60 shows an example of the MatLab code.



```

1 close all;
2 clear all;
3 clc;
4
5 Mop = load('C:\Users\Ellie Heckman\Documents\Masters\Thesis Edit\VRaman Data\1100C 1h x 8\Mo\1100C 1h x 8_Mo_right_22Feb2021_Map1150-1750.txt');
6 Mo1 = load('C:\Users\Ellie Heckman\Documents\Masters\Thesis Edit\VRaman Data\1100C1h x 8 + 1500C1h\Mo\1100C1h x 8 + 1500C1h_Mo_right_Map1150-1750.txt');
7 Mo2 = load('C:\Users\Ellie Heckman\Documents\Masters\Thesis Edit\VRaman Data\1100C1ha8 + 1500C1h x2\Mo_right_Map1.txt');
8 Mo3 = load('C:\Users\Ellie Heckman\Documents\Masters\Thesis Edit\VRaman Data\1100C1ha8 + 1500C1h x3\Mo_right_Map1.txt');
9 Mo4 = load('C:\Users\Ellie Heckman\Documents\Masters\Thesis Edit\VRaman Data\1100C1ha8 + 1500C1ha4\Mo_right_Map1.txt');
10
11 if Mop(1,1) > Mop(end,1)
12     y0 = round(Mop(i,1) + max(Mop(i,1)) + 1);
13     y1 = round(Mo1(i,1) + max(Mo1(i,1)) + 1);
14     y2 = round(Mo2(i,1) + max(Mo2(i,1)) + 1);
15     y3 = round(Mo3(i,1) + max(Mo3(i,1)) + 1);
16     y4 = round(Mo4(i,1) + max(Mo4(i,1)) + 1);
17 else
18     yp = round(Mop(i,1) - min(Mop(i,1)) - 1);
19     y1 = round(Mo1(i,1) - min(Mo1(i,1)) - 1);
20     y2 = round(Mo2(i,1) - min(Mo2(i,1)) - 1);
21     y3 = round(Mo3(i,1) - min(Mo3(i,1)) - 1);
22     y4 = round(Mo4(i,1) - min(Mo4(i,1)) - 1);
23 end
24
25 figure;
26 plot(yp,Mop(i,3),y1,Mo1(i,3),y2,Mo2(i,3),y3,Mo3(i,3),y4,Mo4(i,3),'Linewidth',2);
27 hold on
28 grid on
29 title('Mo Right Scan')
30 ylabel('Intensity')
31 xlabel('Ymu(m)','Interpreter','latex')
32 legend('1100 °C\circ{1h} x 8','1100 °C\circ{1h} x 8 + 1500 °C\circ{1h} x 1','1100 °C\circ{1h} x 8 + 1500 °C\circ{1h} x 2','1100 °C\circ{1h} x 8 + 1500 °C\circ{1h} x 3','1100 °C\circ{1h} x 8 + 1500 °C\circ{1h} x 4');
33 hold off

```

Figure 60: The molybdenum wire right section MatLab code to overlay all five data sets together.

Upon further analysis of the samples, it was seen that the data taken outside of the wire in a region with fibers, showed carbon content. However, when the matrix, outside of the wire, was analyzed, there was no carbon content. The matrix is the portion of the sample that was ceramized from silicon carbide slurry. Figure 61 shows the fiber Raman spectra versus the matrix Raman spectra. The fiber data showed carbon data while the matrix data did not. The fiber carbon intensity is positive because of the carbon peaks being present. This allowed for the software to draw a better line of best fit to determine the area above it, resulting in all of the data being positive. The matrix carbon intensity is negative because of the lack of carbon peaks being present. The lack of carbon peaks in the intensity reading did not allow for the software to develop an accurate line of best fit, thus resulting in variety of the intensity reading and the negative intensity reading. Figure 62 shows the carbon peaks resulting in positive intensity reading. Figure 63 shows the noise in the data resulting in negative intensity reading.

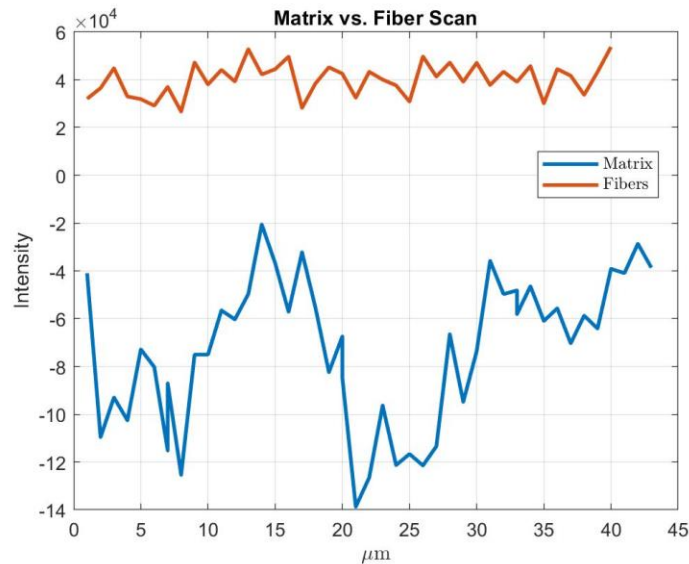


Figure 61: The MatLab generated intensity versus position graph between the fiber and matrix scan showing the differences in the carbon content.

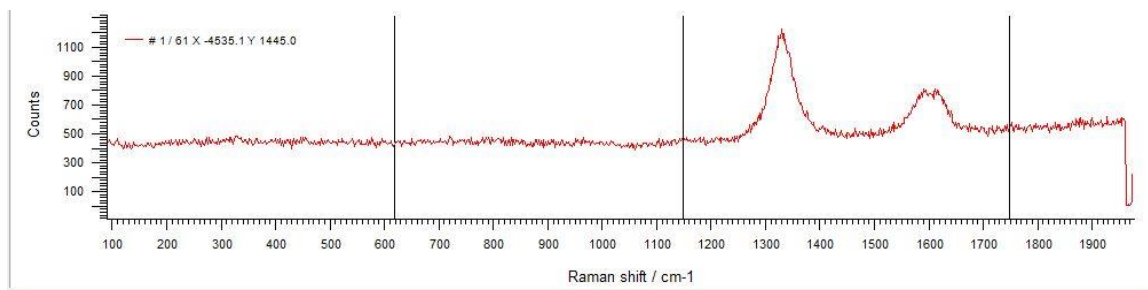


Figure 62: The carbon peaks resulting in positive intensity reading.

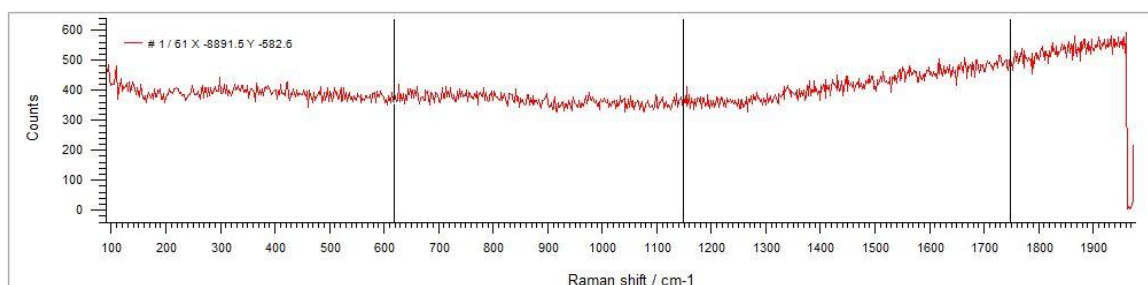


Figure 63: The noise in the data resulting in negative intensity reading.

Figure 61 was added to demonstrate the issues with collecting the carbon data for the samples. If there were not fibers within thirty microns of the metal wire, then there was no carbon content to be interpreted. This resulted in the negative and varying intensity counts. Figure 64 shows two different images taken of the region analyzed during the Raman spectroscopy scan that include fibers, thus resulting in carbon intensity readings. Figure 65 shows two different images taken of the region analyzed during the Raman spectroscopy scan that did not include fibers, thus resulting in no carbon intensity readings. This then caused the line of best fit generated by the software to result in negative intensity readings.

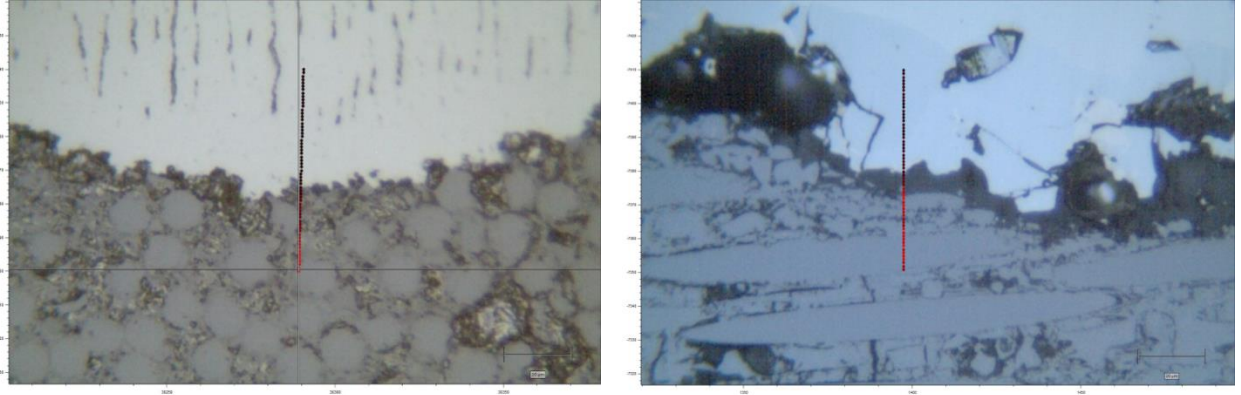


Figure 64: Two different Raman spectroscopy scans that include fiber carbon intensity. The image on the left is the molybdenum wire after $1100^{\circ}\text{C} \times 8$ and the image on the right is the molybdenum wire after $1100^{\circ}\text{C} \times 8 + 1500^{\circ}\text{C} \times 4$.

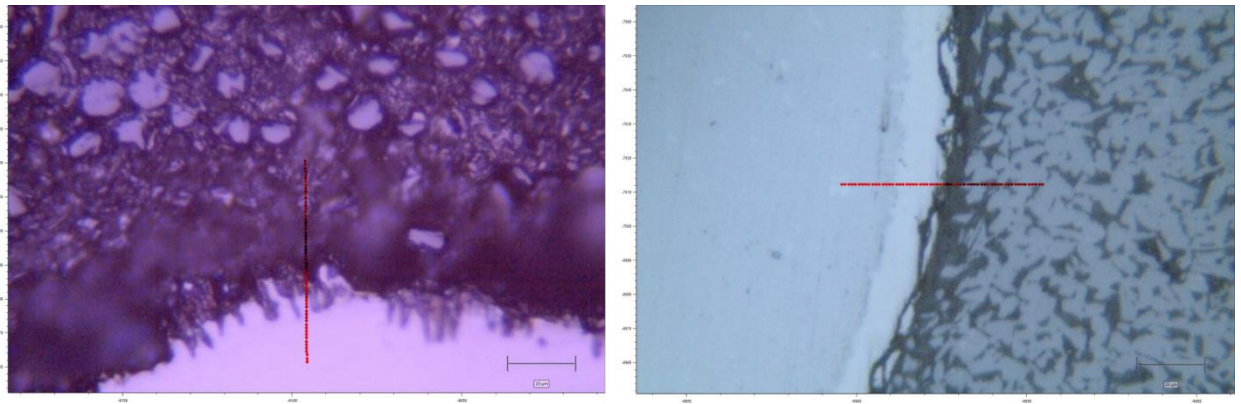


Figure 65: Two different Raman spectroscopy scans that include matrix carbon intensity. The image on the left is the tungsten wire after $1100^{\circ}\text{C} \times 8 + 1500^{\circ}\text{C} \times 2$ and the image on the right is the tantalum wire after $1100^{\circ}\text{C} \times 8 + 1500^{\circ}\text{C} \times 4$.

Figure 66 shows the molybdenum wire bottom region data all overlayed in one graph from the MatLab code. Many of the scans were taken near fiber regions, thus resulting in positive carbon intensity readings. After thirty microns when the intensities all converge at zero, the scan was in the wire, where no carbon was present. This applies to all of the samples analyzed.

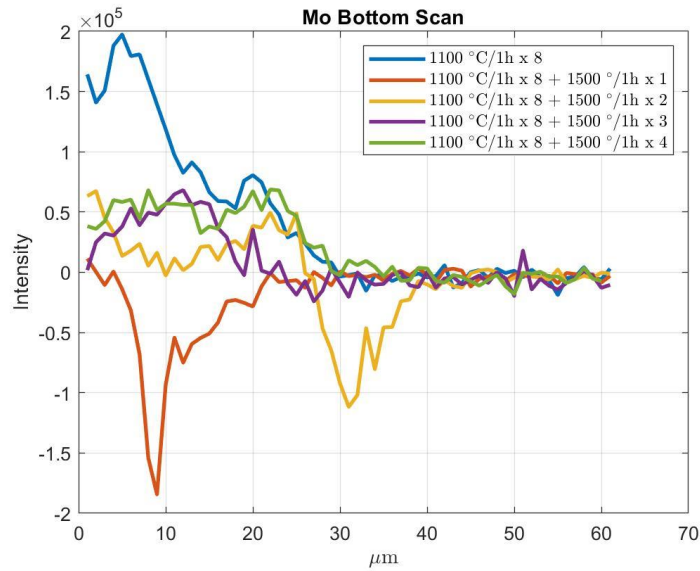


Figure 66: The molybdenum wire bottom region Raman spectroscopy data.

Figure 67 shows the tantalum wire right region data all overlayed in one graph from the MatLab code. Many of the scans were taken near matrix regions, thus resulting in negative intensity readings.

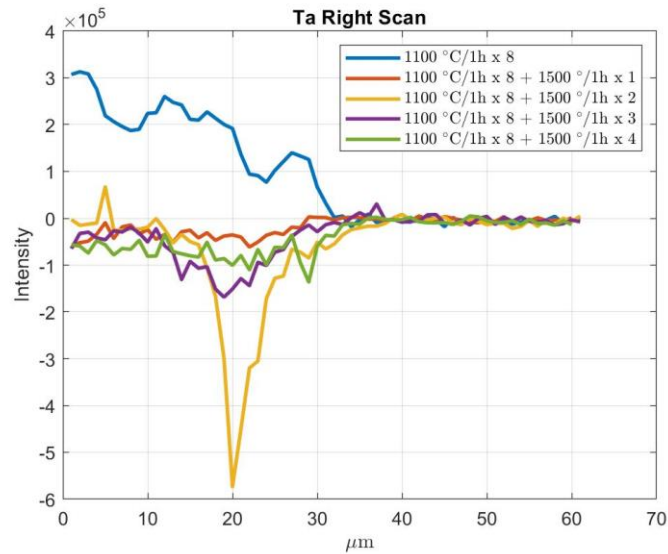


Figure 67: The tantalum wire right region Raman spectroscopy data.

Figure 68 shows the tungsten wire top region data all overlayed in one graph from the MatLab code. These scans were a mix of fiber and matrix regions, resulting in both positive carbon intensities and negative intensities.

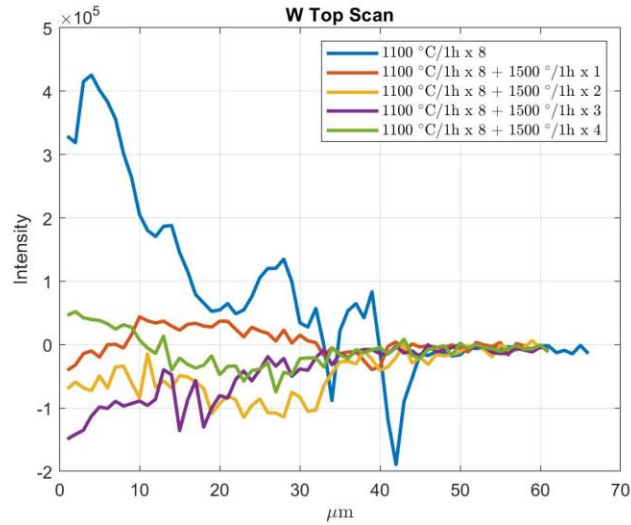


Figure 68: The tungsten wire top region Raman spectroscopy data.

At this point, it is unclear why there is a lack of carbon in the silicon carbide matrix. It is also unclear why the intensity of the carbon signal is so much lower after the additional heating than it is in the 1100°C x 8 sample. The carbon did not migrate into the wires and this is proved by the lack of carbon diffusion seen in the EDS images and the Raman spectroscopy data. Further investigation into these samples is needed to determine where the carbon migrated.

6.3 Conclusion

The tungsten and tantalum samples did not show any signs of diffusion after all four additional heating cycles to 1500°C. There was no evidence of carbon diffusion into either wire seen when analyzing the Raman spectroscopy data. There was also no evidence of silicon diffusion into either wire as seen when analyzing the EDS maps and

linescans. While the tungsten and tantalum wires did not show any signs of diffusion from either silicon or carbon after four additional heating cycles, the molybdenum wire did show signs of silicon diffusion. The silicon diffusion into the molybdenum wire that was seen for all four heating cycles was not uniform. The diffusion zone length varied from location to location within the same wire, making it very difficult to determine the diffusion zone length for each sample with great accuracy. The diffusion zone data obtained from the molybdenum wires was not meaningful under these experiment conditions, thus only allowing for diffusion zone analysis to be done. This did not allow for any diffusion kinetics to be derived but did prove a good basis for where to continue the work in order to determine the diffusion kinetics. It also demonstrated what occurs within the molybdenum, tungsten, and tantalum wires at iterative heating temperatures, emulating an extreme environment for CMC applications.

7. Summary and Conclusions

7.1 Summary

Three different experiments were conducted to determine what occurs when three refractory metal wires are integrated into a ceramic matrix composite. The first set of experiments involved “mock” CMCs with tantalum, tungsten, and molybdenum wires embedded in them. The CMCs were considered to be “mock” CMCs since they did not include silicon carbide fiber weaves. This first set of experiments was investigatory in nature to ensure that the wires could survive different CMC processing temperatures. These temperatures included 900°C, 1100°C, 1300°C, 1500°C, and 1700°C.

The second experiment that was conducted was processing a full CMC, including the silicon carbide fiber weaves. This CMC was processed to 1100°C; it was concluded from the first set of experiments that all three metals survived the PIP processing at 1100°C. Samples were taken after each PIP processing cycle to track any signs of degradation or diffusion within the wires. After fully processing the CMC, there were no signs of degradation or diffusion present in any of the wires. It was then concluded the addition of the fiber weaves did not have any influence on the diffusion or degradation seen.

The third and final experiment that was conducted involved processing a new 1100°C CMC. This CMC was then heated additional to try and induce degradation and diffusion within the wires. This was done to tie in with the first set of experiments that were done, which showed signs of degradation and diffusion. The additional heating also replicated CMC application temperatures. The additional heating cycles done were one hour long

furnace runs at 1500°C. By studying the growth of the diffusion zones and the level of degradation in each wire after each of additional heating, important diffusion and degradation information could be obtained.

7.2 Conclusions

7.2.1 “Mock” CMC

The “mock” CMCs provided information about what occurs within each wire at different temperatures. This was the initial study in this work to determine if the integration of metallic wires into a CMC would even be possible. After determining that it was possible and did not add significant additional cost or time to the processing, the samples were analyzed to see what had occurred at the different processing temperatures. It was determined that all of the wires survived 900°C and 1100°C. At 1300°C and 1500°C, the tungsten wire began to show some signs of degradation around the edges of the wire. The molybdenum wire showed signs of degradation and diffusion. The tantalum wire showed signs of neither degradation or diffusion. At 1700°C, the tungsten and molybdenum wires showed signs of silicon diffusion into the metals and degradation around the edges of the wire. The tantalum wire finally began to show signs of degradation around the edge of the wire, but it did not show any signs of diffusion.

The “mock” CMCs were very important in determining what temperatures the wires could survive. Based on the data and results seen from the “mock” CMC experimentation, it was determined that all three wires should be processed in a full CMC, included the silicon carbide fiber weaves, at 1100°C to see if the addition of the fiber weaves has any influence on the diffusion or degradation of each wire.

7.2.2 1100°C CMC

The 1100°C CMC was analyzed to determine if the addition of the silicon carbide fiber weaves had any influence in the diffusion or degradation of the wires. A sample was taken after each cycles of PIP processing to analysis with an SEM and EDS detectors. This was done to map out any diffusion or degradation that occurred after each step, however there was not any signs of either diffusion or degradation seen. The CMC was fully processed, and all of the wires survived without showing signs of degradation or diffusion. This portion of the experiment showed that tungsten, tantalum, and molybdenum wires could be added to a CMC and processed fully without causing any wire degradation or diffusion. It was seen in the previous “mock” CMC study that diffusion and degradation did occur in the wires at higher temperature, which represent operating temperatures for CMCs. It was determined that the CMC survived at 1100°C but further information was needed to see what happens when the CMC is taken to higher temperatures, representing actual operation of the CMC. To determine what occurs within each wire at higher temperatures, another 1100°C CMC was created and processed. This CMC was then taken to 1500°C in additional heating cycles to see what occurs within the wires.

7.2.3 Diffusion Study

A new CMC, with the three refractory metal wires embedded, was processed to 1100°C with eight PIP processing cycles. The same was then heated to 1500°C for one hour, four different times. A sample was taken after every hour long cycle so the diffusion growth seen in each wire could be measured and related back to the time spent at temperature. SEM and EDS analysis were used to determine the degradation and silicon diffusion in each wire. Raman spectroscopy was used to try and map out the carbon diffusion in the

wires. For the tantalum and tungsten wires, there were no signs of silicon or carbon diffusion. However, the edges of the wires did begin to show signs of degradation after the fourth cycle at 1500°C. There was also no presence of carbon inside the molybdenum wire. The molybdenum wire did have silicon diffusion zones present after the first cycle at 1500°C. The diffusion thickness was non-uniform throughout the wire, resulting in difficulties with accurate thickness averages. The diffusion thickness experienced growth after each iterative cycle. The first to second cycle results in over 25 microns of growth while the second to third only resulted in 4 microns of growth. The third to fourth cycle only showed 5 microns of growth. Due to the diffusion growth slowing, the time dependency of the diffusion zone growth was not able to be determined. The only information that could be obtained from the diffusion zone thickness data was the overall level of degradation of the wires. Further testing to higher temperature and more thickness measurements will allow for the activation energy, diffusion constant, and diffusion rate coefficient could be determined.

7.3 Significance of Results

The results of this experiment are providing initial pathways for determining what occurs to refractory metals when processed with a CMC and taken to higher temperatures. The diffusion of silicon into the wires is important to report due to the new phases forming and degradation of the wires. The new phases that form during the additional higher temperature after processing have not been determined in this work. However, this work will continue directly into being able to determine various diffusion kinetics, such as activation energy, diffusion rate coefficient, and diffusion coefficient, for the phases formed within the molybdenum wires. Further heating to a higher temperature will allow for these diffusion kinetics to be calculated, which will allow for the identification of the

phases formed. This is important to know so the properties can be associated with the CMC.

This work proved that at 900°C and 1100°C, molybdenum, tungsten, and tantalum can be integrated into a CMC and processed without showing signs of degradation or diffusion. Further research is needed to verify if the metals have retained all of their properties that would be beneficial for functional applications, but the lack of degradation and diffusion suggests that the properties remained intact. For molybdenum diffusion and degradation was seen at 1300°C, 1500°C, and 1700°C. This demonstrated that when a processed CMC is taken to higher temperature, the molybdenum wires will experience degradation and have a change in properties. For tungsten, diffusion was not seen until 1700°C, but there were signs of degradation after a few hours at 1500°C. For tantalum, there were no signs of diffusion seen and only slight amounts of edge degradation at 1500°C and 1700°C. This suggests that tungsten and tantalum wires can be embedded in a CMC, processed, and then heated to higher temperatures. The heating to higher temperatures represents the extreme environments that CMCs operate in. Further research is needed to determine when the tantalum and tungsten wires will show full signs of diffusion and what the properties of the metals are, but since the degradation level is low, it can be suggested that the properties remain intact. Continuation of this work will allow for the full integration and operation of CMCs with refractory metallic substrates, taking CMCs from a purely structural component, to one that is also functional.

7.4 Future Work

The work detailed in this thesis was the beginning of this investigation. The work will be continued by Zlatomir Apostolov and other students pursuing graduate degrees. The as

processed 1100°C/8h CMC should be heated in iterative cycles to a temperature higher than 1500°C so the Arrhenius equation can be applied. The Arrhenius equation requires multiple different times and temperatures in order to determine the activation energy and the diffusion constant. By heating the sample to higher temperatures and repeating the same process as described in the third portion of this experiment, more diffusion zone data can be obtained. The samples from the 1500°C iterative heating should also be analyzed again, allowing for more diffusion zone measurements to be taken in hopes of gaining a more accurate diffusion zone thickness for the whole wire. Analyzing specific regions of the wires may also help in determining an average thickness, thus potentially allowing for the time dependency to be determined. One region may have experienced more growth at the first exposure, while another region may have not experienced as much growth. By averaging only one region together, this could potentially resolve the non-uniformity issue currently present.

The next step in continuing this work is going to be determining what phases formed within the molybdenum wire at 1500°C. X-ray diffraction (XRD) analysis is currently being done to try and classify what phases have formed after the additional heating cycles occurred. Multiple different fixtures and accessories are in the process of being purchased to allow for better analysis to occur since the diffusion regions are so small when compared to the overall sample size. A new CMC will also be processed to 1100°C and then taken to higher temperature to try and induce diffusion and degradation present within the tungsten and tantalum wires. The carbon content within the samples is also requiring further analysis to determine where it goes during the additional heating.

Electron backscattered diffraction (EBSD) is being used currently to try and map out the carbon content within the samples.

Once the carbon presence is documented and the phases formed have been identified for all three metals, analysis will be done to determine what the properties the CMC has. For the CMC to be used for other purposes than just structural, the properties associated with each phase are required as they will directly influence the CMC's properties. Once the properties are determined, the CMC will be taken to a point of failure and the properties will be mapped out.

References

1. Alhashmy, H. (2012).
2. Davim, J. P. (2016). *Ceramic Matrix Composites: Materials, Manufacturing and Engineering*. De Gruyter.
3. Unites States of America Patent No. US 6,213,433 B1 , 2001.
4. Bansal, N. P. (2015). *Ceramic Matrix Composites: Materials, Modeling and Technology*. Hoboken, N.J: Wiley.
5. King, D., Apostolov, Z., Key, T., Carney, C., & Cinibulk, M. (2017). Novel Processing Approach to Polymer-Derived Ceramic Matrix Composites. *International Journal of Applied Ceramic Technology*, 15(2), 399–408. doi: 10.1111/ijac.12805
6. Apostolov, Z. D., Heckman, E. P., Key, T. S., & Cinibulk, M. K. (2020). Effects of Low-Temperature Treatment on the Properties of Commercial Preceramic Polymers. *Journal of the European Ceramic Society*, 40(8), 2887–2895. doi: 10.1016/j.jeurceramsoc.2020.02.030
7. Rashid, Muhammad Haroon & Koel, Ants & Rang, Toomas & GÄHWILER, RETO & GROSBERG, MARTIN & Jõemaa, Rauno. (2017). NANOSCALE AND MICROSACLE SIMULATIONS OF N-N JUNCTION HETEROSTRUCTURES OF 3C-4H SILICON CARBIDE. 235-248. 10.2495/MC170241.

8. Shi, Y., Jain, N., & Koch, D. (2018). Investigation and modeling of tensile failure properties of wound ceramic matrix composites. *Composites Part A: Applied Science and Manufacturing*, 114, 316–326. doi: 10.1016/j.compositesa.2018.08.029
9. Nasiri, N. A., Patra, N., Ni, N., Jayaseelan, D. D., & Lee, W. E. (2016). Oxidation Behaviour of SiC/SiC Ceramic Matrix Composites in Air. *Journal of the European Ceramic Society*, 36(14), 3293–3302. doi: 10.1016/j.jeurceramsoc.2016.05.051
10. Dicarlo, J. A., Yun, H.-M., Morscher, G. N., & Bhatt, R. T. (n.d.). SiC/SiC Composites for 1200°C and Above. *Handbook of Ceramic Composites*, 77–98. doi: 10.1007/0-387-23986-3_4
11. Kiser, J. D., Bhatt, R. T., Morscher, G. N., Yun H. M., DiCarlo J. A., & Petko J. F. (2005). SiC/SiC Ceramic Matrix Composites Developed for High-Temperature Space Transportation Applications. NASA Glenn Propulsion Research and Technology.
12. Savitskii, E. M. (1970). *Physical Metallurgy of Refractory Metals and Alloys*. New York: Consultants Bureau.
13. Campbell, F. C. (2008). *Elements of Metallurgy and Engineering Alloys*. Materials Park, OH: ASM International.
14. Garg, S.P Krishnamurthy, N.Venkatraman, M., Venkatraman, M., & Krishnan, R. (Eds.). (1996). *Phase diagrams of binary tantalum alloys*. India: The Indian Institute of Metals.
15. Naidu, S., Sriramamurthy, A., & Rao, P. (1989). *J. Alloy Phase Diagrams* (Vol. 5, Ser. 3).
16. Okamoto, H. Mo-Si (Molybdenum-Silicon). *J. Phase Equilib. Diffus.* 32, 176 (2011).
<https://doi.org/10.1007/s11669-010-9843-0>
17. ICDD PDF 4+ Database, 2020.

18. Zhao, Xingyuan & Togaru, Maanas & Guo, Qianying & Weinberger, Christopher & Lamberson, Leslie & Thompson, Gregory. (2019). Carbon Influence on Fracture Toughness of Niobium Carbides. *Journal of the European Ceramic Society*. 39. 10.1016/j.jeurceramsoc.2019.08.022.
19. Okamoto, H. C-W (Carbon-Tungsten). *J Phs Eqil and Diff* 29, 543–544 (2008). <https://doi.org/10.1007/s11669-008-9396-7>.
20. Guardia-Valenzuela, Jorge & Bertarelli, Alessandro & Carra, Federico & Mariani, Nicola & Bizzaro, Stefano & Arenal, Raul. (2018). Development and properties of high thermal conductivity molybdenum carbide - Graphite composites. *Carbon*. 135. 10.1016/j.carbon.2018.04.010.
21. Brewer, L., Searcy, A. W., Templeton, D., & Dauben, C. H. (1950). High Melting Silicides. *Journal of the American Ceramic Society*. doi:<https://doi.org/10.1111/j.1151-2916.1950.tb14136.x>.
22. Brewer, L., & Krikorian, O. (1956). Reactions of Refractory Silicides with Carbon and Nitrogen. *The Electrochemical Society*. doi:10.1149/1.2430231.
23. Cockerman, B. (1999). The Diffusion Bonding of Silicon Carbide and Boron Carbide Using Refractory Metals. *Conference: ASM Materials Solution 99: International Conference on Joining of Advanced and Specialty Metals*.
24. Ashter, S. A. (2014). Thermoforming of single and MULTILAYER Laminates: Plastic FILMS technologies, testing, and applications. In *Thermoforming of single and multilayer laminates: Plastic films technologies, testing, and applications* (p. 130). Amsterdam: William Andrew is an imprint of Elsevier. <http://dx.doi.org/10.1016/B978-1-4557-3172-5.00006-2>

25. Brandon, D. G., & Kaplan, W. D. (2011). Microstructural characterization of materials. In *Microstructural characterization of materials* (pp. 179-264). Chichester: Wiley.
26. Amer, M. S. (2010). Raman spectroscopy, fullerenes and nanotechnology. In *Raman spectroscopy, fullerenes and nanotechnology* (pp. 43-106). Cambridge, UK: RSC Publishing.
27. Saleh, M. N., Yudhanto, A., Potluri, P., Lubineau, G., & Soutis, C. (2016). Characterising the loading direction sensitivity of 3D woven composites: Effect of z-binder architecture. *Composites Part A*, 90, 577–588. <https://doi-org.ezproxy.libraries.wright.edu/10.1016/j.compositesa.2016.08.028>
28. Oxford Instruments, EDS AZtecLive Map.